NTNU – Trondheim
Norwegian University of
Science and Technology

The Diffuse Synchrotron Radio Background from Normal Spiral Galaxies in the Context of the ARCADE Excess

Lars Einar Stieng

Physics
Submission date: May 2013
Supervisor: Michael Kachelriess, IFY

Norwegian University of Science and Technology
Department of Physics

Abstract

In this thesis, the possibility that synchrotron radiation from cosmic ray electrons in normal spiral galaxies can account for the ARCADE excess is investigated. The ARCADE excess is an excess flux measured in the sky temperature at radio frequencies. It cannot be explained by any of the usual candidates for galactic or extra-galactic emission. Inspired by an article by Fornengo et al., where an origin in synchrotron radiation from electrons produced in dark matter annihilations or decays is proposed, the possibility that conventional synchrotron background from diffuse sources can be responsible is explored. After covering the necessary background material on cosmology, dark matter and radio frequency radiation, a simple model for the total synchrotron background from normal spiral galaxies is presented. The model has some free parameters that control the overall normalization. These parameters include the average synchrotron luminosity of a spiral galaxy and the redshift evolution of these sources. For somewhat optimistic values for these parameters, the model is found able to account for the excess. More constraining experimental data is required to make any conclusive judgments on the viability of the model.

Sammendrag

Denne oppgaven har undersøkt muligheten for at den såkalte 'ARCADE-overflødigheten' kan forklares ved hjelp av synkrotronstråling fra kosmisk stråling (elektroner spesifikt) i normale spiralgalakser . ARCADE-overflødigheten er et ekstra signal i radiofluksen, målt via temperaturen til den mottatte strålingen i dette frekvensområdet. Ulike forklaringer har blitt forsøkt, blant annet den galaktiske og utenomgalaktiske bakgrunnsstrålingen, men ingen av disse kan gjøre rede for overflødigheten. Inspirert av en artikkel av Fornengo m.fl., der en mulig forklaring some foreslås er synkrotronstråling fra elektroner produsert i partikkelreaksjoner med mørk materie, utforskes her muligheten for at vanlig synkrotronstråling fra uoppløste strålingskilder kan være løsningen. Etter å ha dekket nødvendig bakgrunnsstoff om kosmologi, mørk materie og radiostråling, presenteres en enkel modell for den totale synkrotronbakgrunnsstrålingen fra normale spiralgalakser. Modellen har noen frie parametre som påvirker den totale normaliseringen. Dette er blant annet den gjennomsnittlige synkrotronluminositeten til spiralgalakser og rødforskyvningsutviklingen til slike strålingskilder. Hvis noe optimistiske verdier for disse parametrene brukes, er resultatet at modellen kan forklare overflødigheten. Det trengs generelt sett ytterligere eksperimentelle data som kan legge føringer på parametrene, før en kan konkludere sterkere om gyldigheten til modellen.

Acknowledgments

I would like to thank my supervisor, professor Michael Kachelrieß, for all the advice and assistance he has given me during the work on this thesis. He has also helped to arrange several trips to seminars and workshops that have been relevant for the work, and for my professional experience in general. I am grateful for his time and effort.

I would also like to thank my fellow students, who have contributed both through helpful discussions and helpful distractions.

This research has made use of the NASA/IPAC Extragalactic Database (NED) which is operated by the Jet Propulsion Laboratory, California Institute of Technology, under contract with the National Aeronautics and Space Administration.

Contents

Introduction

The presence of dark matter in our Universe gives rise to important questions across several disciplines of modern physics. In Cosmology one might ask about its origin and how it affects the large scale dynamics of the Universe. In Astrophysics one might ask how it coexists with luminous matter inside galaxies, and even solar systems, and how it can be detected in the received extra-terrestrial or extra-galactic flux of radiation. Finally, in particle physics one might ponder its fundamental, quantum nature and whether it can be detected by man-made experiments. So far, the questions far outweigh the answers.

The search for dark matter is conducted in several ways, categorized as either direct or indirect detection experiments. Direct detection experiments can be collider searches – e.g., the Large Hadron Collider (LHC) – or attempts to measure an extra-terrestrial flux of dark matter particles, assuming we are moving through a dark matter halo permeating the galaxy. Indirect detection, both ground based and space based, looks for by-products of dark matter annihilation or decay. This can be either gamma-rays, neutrinos or other Standard Model (SM) particles (or anti-particles). Gamma-ray lines could be smoking guns for dark matter because of low background signals. The other particles would be signs of dark matter if one detects a marked excess compared to what one would expect from astrophysics. In the following, the focus will be on indirect methods. Specifically, the production of electrons and positrons in dark matter annihilations or decays will be considered, the proposed detection method being through the excess synchrotron radiation these would produce when their paths are deflected by galactic magnetic fields.

The purpose of this thesis is to investigate the possibility of a dark matter origin of the 'ARCADE excess'[18, 30, 56, 58], by seeing if this excess could be just normal background synchrotron radiation. The inspiration for the former idea comes from an article by Fornengo et al. [19], which suggests an indirect origin in dark matter, through synchrotron radiation. This motivates exploring whether normal synchrotron radiation from diffuse spiral galaxy sources might be responsible instead. Doing so involves modeling the diffuse background radiation received at Earth, with a focus on radio frequency synchrotron radiation. A comparison of the expected background flux with the excess detected by ARCADE will be done, in order to analyze the possibility that the latter might be a explainable by ordinary synchrotron radiation, rather than synchrotron radiation produced by electrons and/or positrons from particle reactions involving dark matter. In particular, the effect of the variation in flux between the population of normal spiral galaxies, as well as the variation with redshift, will be investigated.

Conventions

In the following, the metric signature $\{+---\}$ will be used. Additionally, the sign of the Riemann, Ricci and Einstein tensors are taken to be, respectively:

$$
\begin{aligned}
+R^{\mu}_{\nu\alpha\beta} &= \partial_\alpha \Gamma^{\mu}_{\nu\beta} - \partial_\beta \Gamma^{\mu}_{\nu\alpha} + \Gamma^{\mu}_{\sigma\alpha}\Gamma^{\sigma}_{\nu\beta} - \Gamma^{\mu}_{\sigma\beta}\Gamma^{\sigma}_{\nu\alpha} \\
+R_{\mu\nu} &= R^{\alpha}_{\mu\alpha\nu} \\
G_{\mu\nu} &= +8\pi T_{\mu\nu}.
\end{aligned}
$$

Natural units, $\hbar = c = 1$, will be used in Chapter 1.

Chapter 1:

The standard cosmological framework and the properties of dark matter

In this first chapter, the well known fundamentals of cosmology and dark matter are discussed. They provide important background and motivation for the work done later, even if some of the topics are not directly relevant to the main questions raised. These topics are included to provide a more complete context.

1.1 Cosmology

Everything in theoretical cosmology is based on, or develops further, the language, ideas and results first derived by Einstein in his general theory of relativity. It is therefore a convenient place to start, particularly in order to motivate some of the results derived later in this section.

1.1.1 Basic General Relativity

The fundamental concept of General Relativity is the connection between the density of energy-momentum and the curvature of spacetime. The approach makes use of the language of tensors and differential geometry, as well as the classical theory of fields. As such, the way to derive the correct equations of motion is to write down the Lagrangian that describes the dynamics of the system, and then extremize the action with respect to the metric. Some familiarity with these topics is assumed in the following.

The total Lagrangian in this case must represent both the dynamics of spacetime itself and that of matter in spacetime. It is hence defined as [39]:

$$\mathcal{L} = \mathcal{L}_{\mathrm{EH}} + \mathcal{L}_{\mathrm{m}},$$

where m stands for matter and EH means Einstein-Hilbert and is given by:

$$\mathcal{L}_{\text{EH}} = \frac{1}{2\kappa} R.$$

Here R is the Ricci scalar, κ is to be determined and the factor $1/2$ is added for later convenience. The Lagrangian for matter is left unspecified for reasons that will become clear below. We then form the action and use the Hamilton principle to find conditions on the Lagrangian,

$$S = \int_\Omega \mathrm{d}^4x \sqrt{|\mathsf{g}|}(\mathcal{L}_{\text{EH}} + \mathcal{L}_{\text{m}}),$$

where g is the determinant of the metric tensor,

$$\delta S = 0,$$

$$\Rightarrow \delta \int_\Omega \mathrm{d}^4x \sqrt{|\mathsf{g}|}(\mathcal{L}_{\text{EH}} + \mathcal{L}_{\text{m}}) = 0. \tag{1.1}$$

Focusing first on the Einstein-Hilbert part, we get

$$\frac{1}{2\kappa} \int_\Omega \mathrm{d}^4x\, \delta(\sqrt{|\mathsf{g}|}\mathsf{g}^{\mu\nu}R_{\mu\nu}) = \frac{1}{2\kappa} \int_\Omega \mathrm{d}^4x\, (\sqrt{|\mathsf{g}|}\mathsf{g}^{\mu\nu}\delta R_{\mu\nu} + \sqrt{|\mathsf{g}|}\delta\mathsf{g}^{\mu\nu}R_{\mu\nu} + R\delta\sqrt{|\mathsf{g}|}).$$

Since $\delta R_{\mu\nu}$ is a tensor, we can calculate it in a frame where the derivatives of the metric, and hence the connection coefficients, vanish:

$$\begin{aligned}
\delta R_{\mu\nu} &= \partial_\lambda \delta\Gamma^\lambda_{\mu\nu} - \partial_\nu \delta\Gamma^\lambda_{\mu\lambda}, \\
\mathsf{g}^{\mu\nu}\delta R_{\mu\nu} &= \partial_\lambda(\mathsf{g}^{\mu\nu}\delta\Gamma^\lambda_{\mu\nu} - g^{\mu\lambda}\delta\Gamma^\nu_{\mu\nu}), \\
\mathsf{g}^{\mu\nu}\delta R_{\mu\nu} &= \partial_\lambda \psi^\lambda.
\end{aligned}$$

In the last line we have used that $\delta\Gamma^\lambda$ is a tensor, even though the connection coefficient itself is not. Promoting to covariant derivatives, we get:

$$\mathsf{g}^{\mu\nu}\delta R_{\mu\nu} = \nabla_\lambda \psi^\lambda.$$

This is a total divergence. It is a common trick to perform a partial integration on these kinds of expressions. Since the variation usually is assumed to be zero when evaluated at the boundary, total divergence terms are seen to vanish when performing partial integrations. Consequently the above term does not contribute. To proceed, we need the identity:

$$\delta\sqrt{|g|} = -\frac{1}{2}\sqrt{|g|}g_{\mu\nu}\delta g^{\mu\nu}.$$

Making use of this, we get:

$$\frac{1}{2\kappa}\int_\Omega d^4x\,\delta(\sqrt{|g|}g^{\mu\nu}R_{\mu\nu}) = \frac{1}{2\kappa}\int_\Omega d^4x\,\sqrt{|g|}(R_{\mu\nu} - \frac{1}{2}g_{\mu\nu}R)\delta g^{\mu\nu}. \tag{1.2}$$

Next, we look at the variation of $\mathcal{L}_m$:

$$\begin{aligned}\delta\sqrt{|g|}\mathcal{L}_m &= \sqrt{|g|}\frac{\delta\mathcal{L}_m}{\delta g^{\mu\nu}}\delta g^{\mu\nu} + \mathcal{L}_m\,\delta\sqrt{|g|},\\ &= \sqrt{|g|}\frac{\delta\mathcal{L}_m}{\delta g^{\mu\nu}}\delta g^{\mu\nu} - \frac{1}{2}\mathcal{L}_m\sqrt{|g|}g_{\mu\nu}\delta g^{\mu\nu},\\ &= \sqrt{|g|}\left(\frac{\delta\mathcal{L}_m}{\delta g^{\mu\nu}} - \frac{1}{2}\mathcal{L}_m\,g_{\mu\nu}\right)\delta g^{\mu\nu}.\end{aligned} \tag{1.3}$$

Since the variation of the metric is arbitrary, (1.1), (1.2) and (1.3) give:

$$G_{\mu\nu} \equiv R_{\mu\nu} - \frac{1}{2}g_{\mu\nu}R = -2\kappa\left(\frac{\delta\mathcal{L}_m}{\delta g^{\mu\nu}} - \frac{1}{2}\mathcal{L}_m g_{\mu\nu}\right) \equiv 2\kappa\frac{1}{2}T_{\mu\nu},$$

where $G_{\mu\nu}$ is called the Einstein tensor and $T_{\mu\nu}$ is the energy-momentum tensor. This simplifies to:

$$G_{\mu\nu} = \kappa T_{\mu\nu},$$

with κ given by the Newtonian limit [39]:

$$G_{\mu\nu} = 8\pi G_N T_{\mu\nu}. \tag{1.4}$$

The above definition of the energy-momentum tensor is consistent with the one in classical field theory, as well as automatically symmetric. It is also possible – that is, consistent with general covariance – to add a 'cosmological constant' term to the Einstein equation, as historically Einstein did to get a static Universe. Having the form of vacuum energy, this is often done in modern cosmology in order to account for dark energy. Adding this term, the Einstein equation becomes:

$$G_{\mu\nu} = 8\pi G_N T_{\mu\nu} + \Lambda g_{\mu\nu}, \tag{1.5}$$

where the parameter Λ is called the cosmological constant and provides energy density associated with the vacuum.

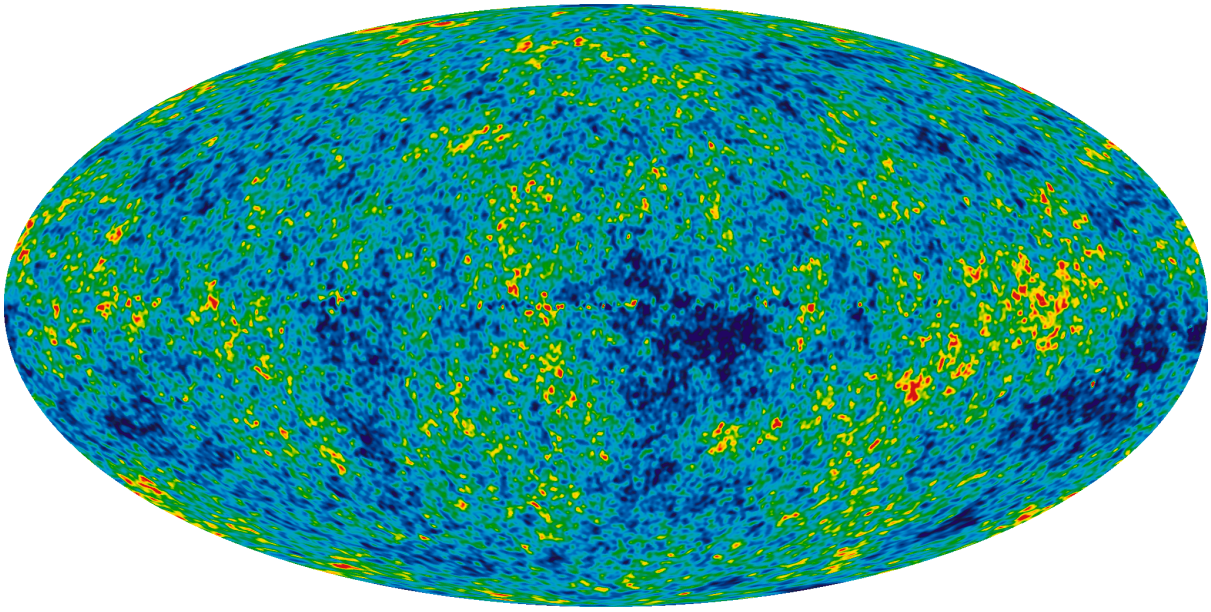

Figure 1.1: Temperature map of the CMB from the WMAP 9 year data, showing the fluctuations present in the very early Universe. Taken from [40].

1.1.2 The standard cosmological model

The standard model of cosmology is based on what is called the hot Big Bang theory, which says that initially the Universe was in a state of infinite density and curvature, a singularity. At some point, an 'explosion' (dubbed the Big Bang) occurred, which caused spacetime to expand. The energy contained within then started to cool and formed the fundamental particles we know today. Although physics breaks down at the singularity, modern cosmology has been able to make predictions about the dynamics of the very early Universe, going as far back as 10^{-43}s after the Big Bang [31].

To make a model of the Universe, one needs to make assumptions about the large scale structure, ideally based on, or consistent with, observations. The common assumptions are those of homogeneity and isotropy above a certain distance scale, usually on the order of 100 Mpc. Put in another way, this is the idea that we do not occupy a special place in the Universe, often called the 'Cosmological Principle'. Clearly, this is not the case on smaller distance scales, as we observe matter to be clustered together by gravity in the form of solar systems, galaxies and clusters of galaxies. However, these structures start to smooth out when considering the Universe as a whole. Observational support for this is found in maps of the Cosmic Microwave Background (CMB), see Figure 1.1. This is the leftover radiation from the moment when the Universe became translucent to photons. Currently, these photons have cooled to a temperature of 2.73 K, and the large degree of isotropy observed is consistent with standard cosmology. Some anisotropies are in fact observed in the CMB, but this is to be expected. Otherwise, the massive structures in the Universe would not have formed.

Lastly, as a consequence of the Big Bang, one would expect that the Universe is non-static. Non-static in this context means that the Universe is either presently expanding, or that it was expanding in the past and is now contracting. This is in fact what motivated the idea of the

Big Bang in the first place. Edwin Hubble noticed in the 1920s that distant galaxies appeared consistently red-shifted compared to what one would expect in a static Universe. Additionally, earlier work by Georges Lemaître had already suggested that the Universe might be expanding, and in fact proposed the idea of the initial singularity itself. Thus the standard model of cosmology says that we are living in an expanding, homogeneous and isotropic Universe, which started as a singularity and evolved for billions of years into the present state.

1.1.3 The FLRW metric and dynamics

To obtain quantitative models that produce the observed dynamics of the Universe, one needs a metric which is a solution to the Einstein equation for a given energy-momentum tensor. With the above assumptions about the large scale structure of the Universe, one common choice for calculations in cosmology is the Friedmann-Lemaître-Robertson-Walker (FLRW) metric. It is the only choice for a homogeneous and isotropic Universe, with a time-dependent constant curvature spatial component. In standard notation, it is given by:

$$\mathrm{d}s^2 = \mathrm{d}t^2 - a(t)^2 \left[\frac{\mathrm{d}r^2}{1 - kr^2} + r^2(\mathrm{d}\theta^2 + \sin^2(\theta)\mathrm{d}\phi^2) \right]. \tag{1.6}$$

Here $a(t)$ is the normalized scale factor, which determines the expansion, and k is a constant with values {-1,0,+1}, giving the sign of the curvature of the spatial 3-surface (hyperbolic, flat and spherical respectively). A common and very useful energy-momentum tensor for this Universe is that of a perfect fluid with pressure p and density ρ, i.e.:

$$T^{\mu\nu} = (\rho + p)u^\mu u^\nu + pg^{\mu\nu}, \tag{1.7}$$

where $g^{\mu\nu}$ is the metric tensor and u is the four-velocity of the fluid. By conservation of energy-momentum:

$$\nabla_\nu T^{\mu\nu} = 0,$$

we get (from the $\mu = 0$ component) [31]:

$$\mathrm{d}(a^3\rho) = -p\mathrm{d}a^3.$$

This expresses the first law of thermodynamics for an expanding (fluid) Universe. Using an equation of state:

$$p = w\rho,$$

where w is assumed to be time-independent, yields an expression for the time evolution of the density:

$$\rho \propto a^{-3(w+1)}. \tag{1.8}$$

There are several interesting cases to look at here. In a Universe dominated by radiation, here meaning relativistic particles and photons, as is believed to be the case in the early Universe [31], one has $w = 1/3$ and thus:

$$\rho \propto a^{-4}.$$

For a matter dominated Universe, $w = 0$ and:

$$\rho \propto a^{-3}.$$

Finally, for a Universe where most of the density is in the form of vacuum energy, $w = -1$ and:

$$\rho \propto \text{constant}.$$

To get more information, another equation is needed. Using the 0-0 component of (1.4), as well as (1.6) and (1.7), gives:

$$\frac{\dot{a}^2}{a^2} + \frac{k}{a^2} = \frac{8\pi G_N}{3}\rho, \tag{1.9}$$

which is known as the Friedmann equation. Defining the Hubble parameter as:

$$H \equiv \frac{\dot{a}}{a}, \tag{1.10}$$

and dividing the Friedmann equation by this factor, produces:

$$\frac{k}{H^2R^2} = \frac{\rho}{3H^2/8\pi G_N} - 1. \tag{1.11}$$

This motivates defining:

$$\Omega \equiv \frac{\rho}{\rho_C}, \qquad \rho_C \equiv \frac{3H^2}{8\pi G_N},$$

as the relative density and the critical density respectively. It is evident that the critical density is that which gives exactly $k = 0$, a flat Universe, while values for the density above and below the critical one give a spherical and hyperbolic Universe, respectively. It is important to note that both Ω and ρ_C are time-dependent, changing as the Universe expands.

It can also be beneficial to define a physical radius of curvature of the Universe as [31]:

$$R_{\text{curv}} \equiv R|k|^{-1/2} = \frac{H^{-1}}{|\Omega - 1|^{1/2}},$$

where H^{-1} in this context often is called the Hubble radius.

For a flat Universe, one can get expressions for the scale factor by combining (1.9) and (1.8), and then solving the resulting differential equation to get:

$$a(t) \propto t^{2/3(1+w)}. \tag{1.12}$$

This gives $a \propto t^{1/2}$ for radiation, $a \propto t^{2/3}$ for matter and $a \propto \exp(H_0 t)$ for vacuum energy. The last case requires solving the differential equation given by (1.9) and (1.8) again, for the special case $w = -1$. H_0 is the Hubble parameter evaluated at the current time, usually referred to as the Hubble constant.

1.1.4 Obstacles of the standard model of cosmology

The standard model, sometimes referred to as the concordance model, is well suited for describing the current state of the Universe. Still it has a few serious weaknesses in terms of describing how the Universe came to be in such a state. Among the more important problems are the horizon problem, the problem of small scale inhomogeneity, the flatness problem, the unwanted relics problem and the cosmological constant problem [31]. Only the first four have a commonly accepted solution, which will be outlined below, while the last one remains one of the big unsolved problems of physics and motivates the search for quantum theories beyond the Standard Model of particle physics. These theories can either deal with the cosmological constant as vacuum energy in a typical quantum field theory context (like, e.g., Supersymmetry), or through ways that also shed light on the small scale nature of spacetime and gravity (like, e.g., String Theory).

The horizon problem. The horizon problem [39] is an issue arising from the present level of homogeneity in the Universe. Specifically, this is hard to reconcile with the fact that the Universe is made up of regions that were causally disconnected, i.e. could not have affected each other, at recombination ($z \approx 1100$). In fact, at that time the present Hubble volume comprised roughly 10^5 causally disconnected regions [31]. If no light signal could have propagated between these areas, then there is seemingly no way for the present level of observed homogeneity to occur. To see this, one introduces the notion of horizon distance, which in a flat FLRW-metric is given by:

$$\mathrm{d}_H(t) = a(t) \int_0^t \frac{\mathrm{d}t'}{a(t')}.$$

Obviously, the horizon distance depends on the model one uses – different for, e.g., matter

dominated and radiation dominated Universes – however, in the concordance model it is roughly equal to the Hubble radius:

$$\mathrm{d}_H(t) \approx H(t)^{-1}. \tag{1.13}$$

The large scale homogeneity of our horizon volume (or as (1.13) suggests, Hubble volume) is, as mentioned earlier, well supported by temperature measurements of the CMB. Thus we are left with a puzzling question of why this 'smoothness' of the Universe is so prevalent, when there is no mechanism to account for it.

Small scale inhomogeneity. As discussed above, the Universe is quite homogeneous on large scales. However, as is well known, there is a lot of structure on small scales which is not evenly distributed. From the level of planets and moons to clusters of galaxies, granular structure is ubiquitous. Again, it is unclear how this came to be. In general such structure can arise due to density perturbations in the matter distribution. If a perturbation in the density causes small scale clumping, then gravity will tend to reinforce the effect and larger structures may form. The problem with this mechanism as the origin of small scale homogeneity is as before one of horizons and causal disconnectedness. The size of the density perturbations at decoupling is bounded by the temperature fluctuations in the CMB:

$$\frac{\delta\rho}{\rho} \propto \frac{\delta T}{T}.$$

There is already a problem present in a Universe without dark matter, because inhomogeneities from baryons cannot form until after decoupling due to interactions with photons. This would make forming the present large scale structures impossible. Luckily dark matter can accommodate this, as dark matter can induce inhomogeneities as early as the time of the matter-radiation equilibrium of the energy density. It is also important to note that the primordial power spectrum of these density fluctuations is constant. This is property is usually called scale invariance. Additionally, the density perturbations grow linearly in the matter dominated Universe until $\delta\rho/\rho \approx 1$. The problem faced in standard cosmology then, is that perturbations corresponding to galaxies and larger structures are at a scale lying outside the horizon in the early universe. It is consequently not possible to seed the initial perturbations required for the inhomogeneity in the present Universe. In this way, the standard cosmological model fails to account for both large scale homogeneity and small scale inhomogeneity, particle horizons being the culprit in either case.

The flatness problem. Another problem arises from the high degree of spatial flatness, or, said in another way. the closeness of Ω to unity. At the current time this poses no difficulty. However, extrapolating backwards towards the Planck epoch (10^{-43}s), some trouble appears. As previously noted, Ω is time-dependent. Therefore, it becomes increasingly close to unity when evaluated at earlier times (based on the current value). Additionally, this means that the radius of curvature becomes considerably larger than the Hubble radius. Then, recovering our current Universe becomes a fine-tuning problem. Slight variations in the energy density give very different cosmological evolutions, many resulting in either a quick recollapse or a very

cold, low density Universe. Once again the concordance model fails to explain why it is so difficult to have the Universe evolve from an early state into one with the present values for the cosmological parameters.

Problem of unwanted relics. In non-abelian, unified gauge theories, it has been shown [48, 62] that production of very heavy magnetic monopoles is permitted. It has also been shown that these particles could have been produced in excess in the early Universe [70, 49]. However, no such particles have been observed, and the amount produced would have a noticeable effect on the total energy density. One could argue that since the existence of these relics depends upon the reality of grand unified theories (GUTs), the particles could easily be avoided by abandoning GUTs, but there are other reasons that one might wish to keep them. These particles would also be stable and could therefore be a dark matter candidate (see later discussion for details on dark matter). However, if these relics are to exist, there still needs to be a mechanism that can explain why their abundance is much lower than predicted. This standard cosmology cannot do.

The cosmological constant problem. Finally, the cosmological constant problem is one of the big problems encountered when one attempts to combine general relativity with quantum field theory. As we have seen, the Einstein equation allows a cosmological constant term, which behaves like a vacuum energy. There is also no fundamental symmetry in the Standard Model of particle physics that would disallow it. In fact, vacuum energy is a common constituent of quantum field theories and is predicted to have a large contribution. This is then contrasted with the fact that the amount of vacuum energy in the Universe is so small. Because of the effect it has on the dynamics of the Universe (see discussion beneath (1.12)), the total energy density of vacuum energy must be of the order of the critical density. The presently estimated value based on observations is actually slightly less than this. A quite puzzling fact, since this value misses the one predicted by quantum field theory by more than 100 orders of magnitude. The way to see this, is by assuming that the Standard Model is valid up to the Planck scale. Using a cutoff regularization, vacuum energy should then be of the order of the Planck mass to the fourth power, that is $\sim (10^{19}\text{GeV})^4$. Not undeservedly so, this is considered one of the great failures of modern physics.

1.1.5 Remedy in the inflationary paradigm

The solution to these problems (except the last) is the idea of inflation [24, 34, 1], which proposes an early phase of the Universe where spacetime expands very rapidly. The proposed mechanism for this is through the dynamics of a scalar field called an inflaton, the details of which will be skipped for brevity. The important point is that at some early time right after the Big Bang, vacuum energy dominated the total energy density of the Universe. As discussed beneath (1.12), this gives an exponentially increasing scale factor. The Universe then experienced a period of rapid expansion, called a de Sitter phase. During this phase, there is a 'supercooling' of each region of space, keeping the entropy constant [31]. At some point, the inflaton field will decay and create other particles that it interacts with and loses energy to. As these other particles thermalize, the Universe will reheat and entropy will increase by vast amounts. The evolution of the Universe then proceeds according to the concordance model.

This solves both the horizon and the flatness problems. It explains the horizon problem by ensuring that the patches of a size on which one might expect homogeneity before the inflationary epoch, grow sufficiently during inflation to be much larger than our current particle horizon (about 10^{56} times). In other words, the entire observable Universe was in causal contact at early times. The flatness problem is accommodated by the fact that as the curvature radius increased rapidly during inflation, the total energy density did not. It in fact remained constant. Thus one would expect the radius of curvature to be much larger than the Hubble radius, and hence that the Universe is flat, i.e., Ω being very close to 1.

The problem of small scale inhomogeneity is not immediately solved, but can be nevertheless accommodated. This is achieved by observing that quantum fluctuations of the inflaton field can provide the means for the creation of structure on cosmologically relevant scales [31]. The quantum fluctuations create metric perturbations that, when interacting with the matter distribution after inflation, cause density perturbations leading to clustering, and eventually (local) large scale structure.

Additionally, inflation can dilute the number density of super-heavy monopoles if they are only produced before or during inflation. This will be the case if the temperature of GUT symmetry breaking is reached prior to the end of inflation, and the reheating temperature is low enough that the monopoles are not produced in significant numbers. Alternatively, certain formulations of inflation [34] do away with the production of monopoles altogether. Hence, whether it is desirable to lessen the abundance or stop their production completely, inflation can accommodate the unwanted relics problem.

1.1.6 Extending the concordance model

After the idea of inflation, another big change in cosmology was soon to come. In the late 1990s , measurements of supernovae indicated that the expansion of the Universe was in fact accelerating [47, 50]. The explanation: some kind of cosmological constant. This and other alternative explanations for the accelerated expansion have since been termed 'dark energy'. This name coming from their similarity with dark matter in being invisible to detection save for the influence it has on the geometry of the Universe. Since then, experiments have made it clear that we seem to live in a flat Universe, with most of the energy density in the form of dark matter and dark energy. In particular, only about 26% of the total energy density is in the form of matter.

The concordance model of cosmology, with or without inflation, extended to include dark energy in the form of a cosmological constant and dark matter as the main constituents of the Universe is referred to as ΛCDM, or also just as the concordance model. The Λ meaning cosmological constant and CDM being short for cold dark matter (to be outlined below). The important parameters of ΛCDM are given in Table 1.1. This thesis will assume these values for the fundamental constants in cosmology, and use them in all relevant calculations. The model is fairly robust with regard to most modern observations of the Universe, but lacks an explanation for some of the fundamental physics underlying the large structure, such as the nature of dark energy and dark matter.

Table 1.1: Parameters of ΛCDM [26].

Parameter	Symbol	Value
Hubble constant (normalized)	$h \equiv H_0/(100\ \mathrm{km\ s^{-1}Mpc^{-1}})$	$h = 0.72 \pm 0.03$
Total matter density	Ω_m	$\Omega_\mathrm{m}h = 0.133 \pm 0.006$
Baryon density	Ω_b	$\Omega_\mathrm{b}h = 0.0227 \pm 0.0006$
Cosmological constant	Ω_Λ	$\Omega_\Lambda = 0.74 \pm 0.03$
Radiation density	Ω_r	$\Omega_\mathrm{r}h = 2.47 \times 10^{-5}$

1.2 Dark Matter

With the basic tools of calculation in order, one may proceed to the main motivation for the thesis, namely dark matter. While not directly linked to the actual work done later, it provides a context within which the main questions are relevant to ask. It is therefore important to get a good, if brief, overview of the main elements of the underlying theory. To do so, is to introduce both how dark matter was first suggested and the present state of knowledge.

1.2.1 Evidence

It has long been speculated that the visible, or luminous, matter in the Universe is only a fraction of the total matter density. In early work, Fritz Zwicky [71] suggested that based on estimates of the virial mass of the Coma cluster of galaxies, there must be some unseen matter component in these galaxies. Zwicky referred to it in his paper as 'dark matter' ('dunkle Materie'). The virial mass of a galaxy or cluster can be estimated in the following way:

Assume that the system is gravitationally bound, then the virial theorem:

$$2\langle T\rangle + \langle V\rangle = 0,$$

where T and V are the kinetic and potential energies and the brackets indicate time-average, applies. Using this and the usual expressions for T and V in a gravitational system gives an estimate, called the virial mass, of the total mass of the system [11]:

$$M_{vir} = \frac{2\langle v^2\rangle R_{hms}}{G_N}.$$

Here, R_{hms} is the harmonic mean separation of the individual masses of the system, the former being the inverse of the mean of inverse distances. Measuring the velocities and positions of the system constituents, the mass of the system can be deduced. In this way, Zwicky arrived at

a lower bound on the mass of the Coma cluster. This bound far exceeded that which could be deduced from the luminosity.

Some decades later, Vera Rubin and Kent Ford investigated the rotation curve of the Andromeda galaxy [52] and later, with Norbert Thonnard, the rotation curves of 10 high luminosity spiral galaxies [53]. In both cases they found that the rotation curves were flat, as opposed to decreasing. The latter being what one would expect if most of the mass of the galaxies were contained within the luminous region. Combined with independent suggestions that a large component of the matter in galaxies might be within extended halos [43, 44], this gave rise to the modern idea of dark matter.

A rotation curve, see Figure 1.2, is a measure of the velocity distribution of stars in a galaxy as a function of radial distance to the center. One measures this velocity by studying the Doppler shifted spectral lines of either stars (inner galaxy) or HI-clouds (outer galaxy). It is assumed that these objects, at position r and with velocity $v(r)$, follow an approximately circular orbit. Then one can take advantage of the fact that their Newtonian gravitational interaction with the matter inside a sphere with radius $< r$ drives this motion. This yields:

$$\frac{M(r)G_N}{r^2} = \frac{v(r)^2}{r},$$

where $M(r)$ is the mass inside the sphere of radius r. Hence:

$$v(r) = \sqrt{\frac{M(r)G_N}{r}}.$$

Assuming that the density of stars is constant, one has:

$$M(r) = \rho\frac{4\pi}{3}r^3 \Rightarrow v(r) \propto r,$$

inside the region where most of the mass is contained. Outside, where $M(r)$ should be roughly constant with respect to the radial distance, this becomes:

$$v(r) \propto r^{-1/2}.$$

This suggests that outside the region where most of the stars in the galaxy are observed to be, the velocity should fall off with increasing distance. However, this was not observed in the work of Rubin and her collaborators. Rather, the velocity was found to be constant with distance when moving beyond the optical disk. These observations lead to the speculated existence of an extended, massive halo filled with some kind of dark matter.

In both of the above cases (Coma cluster and rotation curves) an important tool is the mass-to-luminosity ratio M/L, which if there were no dark matter present should be roughly 1. However, the existence of dark matter was inferred when the ratio was found be significantly larger than that.

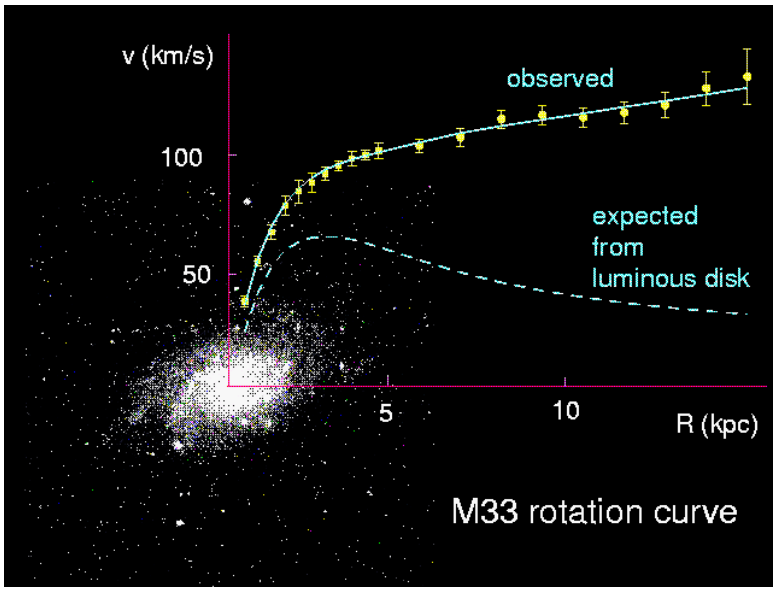

Figure 1.2: Rotation curve of M33 superimposed on image of the galaxy [54].

There have been attempts to explain these discrepancies in other ways. The most notable being Modified Newtonian Dynamics (MOND) [37, 38] and its extension, Tensor-Vector-Scalar gravity (TeVeS) [6]. MOND postulates that Newtonian gravity should be adjusted for small accelerations in such a way as to explain why the rotation curves would flatten far from the source (weak fields), but recovering the normal behavior for larger accelerations (stronger fields). TeVeS is a similarly motivated theory that accommodates relativistic cases (explaining for instance gravitational lensing and large scale cosmology) while reducing to MOND in the non-relativistic limit. Whereas MOND fails to explain structure formation and the much celebrated 'smoking gun' of dark matter, the 'Bullet Cluster' (see figure 1.3) [15], TeVeS can, with some work, actually account for both. However, it fails to explicate the CMB anisotropy and certain considerations from Big Bang Nucleosynthesis (BBN).

It seems clear then, that the Universe consists of a large amount of unknown matter. This non-luminous matter component must be elucidated in order to form a complete cosmological model, as well as gaining an understanding of the constituency and inner workings of our own galaxy.

1.2.2 Candidates

However, astrophysics and cosmology can only take us so far. Although both provide evidence for its existence and some criteria for its fundamental nature (mostly by excluding certain kinds of matter), a particle physics approach is needed to ascertain the true properties dark matter may possess. The main characteristic of dark matter is of course that it is 'dark', in the sense that it does not interact noticeably with photons and hence that these particles must be electrically neutral [64]. One way to separate candidates, is whether they move at relativistic or non-relativistic speeds, usually termed 'hot' and 'cold'. One long held possibility for hot

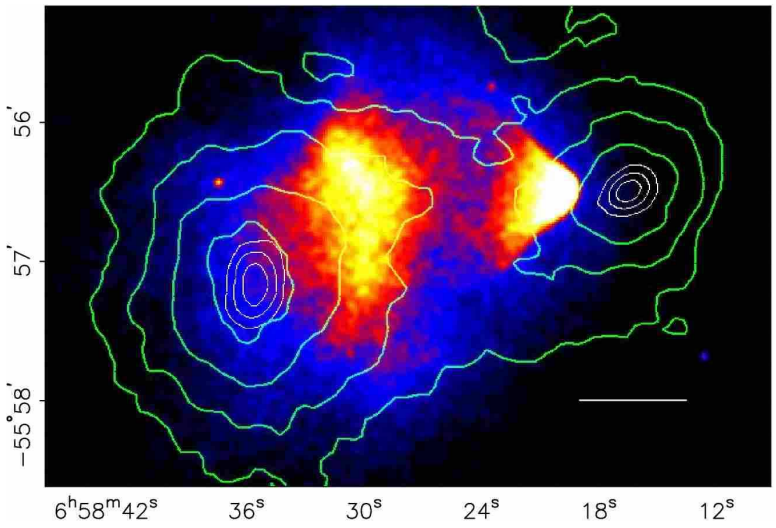

Figure 1.3: Image of the Bullet cluster from [15]. The red and yellow colors signify gas clouds detected by X-ray signals, while the blue shows dark matter detected by gravitational lensing.

dark matter was neutrinos. However, neutrinos have been excluded by the upper bounds on their mass giving a far too low relic density [9]. Additionally, hot dark matter cannot be the main component of dark matter in the Universe. There are several reasons for this, but the main one is that hot dark matter gives a too low power spectrum for structure on small scales. In other words, hot dark matter is not consistent with the current theories about structure formation. As a consequence, cold dark matter must be responsible for the main contribution to the total dark matter density. Beyond these constraints, particle physics gives several possibilities for the exact properties of dark matter:

Baryonic dark matter. From the above, there is nothing that rules out a baryonic dark matter candidate. In fact, several have been proposed, most notably a type called Massive Compact Halo Objects (MACHOs). This category includes brown dwarfs, large Jupiter-like planets, black holes, white dwarfs and neutron stars [23, 31]. As with neutrinos these objects make some contribution to the dark matter density, but cannot be a major part. The reason for this is that BBN and the CMB place upper bounds on the baryon fraction of the total matter density. These bounds are far too low for baryons to make up a significant component (as indicated by the value given in Table 1.1).

WIMPs. The most popular of the non-baryonic candidates is the weakly interacting massive particle (WIMP). This is a general class of particles with the property that they in addition to having noticeable, large scale gravitational interaction, interact weakly by e.g., neutral currents. In this way, they may be detectable through elastic scattering off atomic nuclei. Assuming that we are surrounded by a dark matter halo, the solar system should be moving through a 'wind' of WIMPs that then collide with local baryonic matter. A WIMP event could then be detected by the recoil of nuclei, causing ionization, radiation or lattice vibrations. A big challenge here, is distinguishing between a WIMP event and any other event with the same end result. There is hope that this could be remedied by the changing 'wind speed' of the WIMPs, caused by the

seasonal variation in the direction of the earth's movement around the sun. Another way of detection, which is somewhat related to the one discussed in this thesis, is through gamma rays produced in particle-antiparticle annihilations. This kind of indirect detection could potentially give a direct measurement of the WIMP mass due to the unique gamma ray energy (a line in the spectrum). Complications here arise due to the fact that gamma rays may not be the only primary product of this reaction, or in fact not part of the primary product at all. Rather, it could be an end-product of a jet or other chains of reactions. This gives a more diffuse spectrum of possible gamma ray signals to check. Further complications arise due to the fact that any gamma ray signal must be distinguished from the plethora of background signals.

The most attractive feature of the WIMPs is their production mechanism. Produced thermally before the BBN-era, the fact that they interact weakly seem to give the desired order of magnitude for the relic density, compared to what we should expect from modern observations. Thermal production in the early Universe works in the following way. One assumes that before some time, the WIMP existed in chemical equilibrium with SM particles in a plasma of particles and anti-particles. That is, the reaction rate for the process where one type produces the other is equal in both directions. A requirement for this, is that the rate is faster than the expansion of the Universe:

$$\Gamma > H, \tag{1.14}$$

where H is the Hubble parameter, and the rate is given by:

$$\Gamma_{\text{ann}} = n_{\text{eq}} \langle \sigma_{\text{ann}} v \rangle. \tag{1.15}$$

Here 'ann' stands for annihilation, σ denotes the cross section, n_{eq} is the equilibrium number density of WIMPs and v is the relative velocity. Note that the brackets indicate that a thermal average has been done over the distribution of WIMP particles. As the Universe expanded, the number density, and hence the rate, decreased. Additionally, because this caused a decrease in temperature and hence the kinetic energy available, fewer and fewer particles could be produced. This lowered the equilibrium number density (the equilibrium still held). At some point, often referred to as the 'freeze-out' time, the rate became slower than the expansion and the WIMPs then decoupled from the SM particles. As a consequence, their number, or abundance, at that point was held fixed, while their density evolved due to the expansion only (i.e. strictly inversely with volume). The density at freeze-out is called relic density. For the WIMPs this has the desired order of magnitude to account for the amount of dark matter today, adjusted for the expansion of the Universe since freeze-out.

The progression of the WIMP density into the present value is governed by the following two equations, giving the time-evolution of the number density and total entropy density respectively:

$$\frac{\mathrm{d}n}{\mathrm{d}t} = -3Hn - \langle \sigma_{\text{ann}} v \rangle (n^2 - n_{\text{eq}}^2) \tag{1.16}$$

$$\frac{\mathrm{d}s}{\mathrm{d}t} = -3Hs. \tag{1.17}$$

The first (and only for equation (1.17)) term on the right hand side of the two equations comes from the expansion of the Universe, the factor 3 because of expansion in all spatial directions, while the second term in (1.16) takes into account the effect of annihilation and creation. It is common [8] to combine these equations by defining $Y \equiv n/s$ and $x \equiv m/T$, where T is the photon temperature. This gives:

$$\frac{\mathrm{d}Y}{\mathrm{d}x} = \frac{1}{3H}\frac{\mathrm{d}s}{\mathrm{d}x}\langle\sigma_{\mathrm{ann}}v\rangle(Y^2 - Y_{\mathrm{eq}}^2). \tag{1.18}$$

From (1.11) with $k = 0$, we have:

$$H^2 = \frac{8\pi G_N}{3}\rho.$$

Using instead the Planck mass $m_{Pl} \equiv G_N^{-1/2}$, gives:

$$H^2 = \frac{8\pi}{3m_{Pl}^2}\rho.$$

To proceed, the energy density and entropy density can be expressed as functions of T in the following way:

$$\rho = \frac{\pi^2}{30}g_{\mathrm{eff}}(T)T^4,$$
$$s = \frac{2\pi^2}{45}h_{\mathrm{eff}}(T)T^3,$$

where g_{eff} and h_{eff} are the effective degrees of freedom for the two quantities. With a final definition of the degrees of freedom parameter as:

$$g_*^{1/2} \equiv \frac{h_{\mathrm{eff}}}{g_{\mathrm{eff}}^{1/2}}\left(1 + \frac{T}{3h_{\mathrm{eff}}}\frac{\mathrm{d}h_{\mathrm{eff}}}{\mathrm{d}T}\right),$$

a simplified expression for (1.18) can be found:

$$\frac{\mathrm{d}Y}{\mathrm{d}x} = -\left(\frac{45}{\pi m_{\mathrm{Pl}}^2}\right)^{-1/2}\frac{g_*^{1/2}m}{x^2}\langle\sigma_{\mathrm{ann}}v\rangle(Y^2 - Y_{\mathrm{eq}}^2).$$

This can be solved numerically. In particular, one uses $Y = Y_{\mathrm{eq}}$ when $x \simeq 1$ as initial condition. This gives the present value, Y_0, which can be used to find the contemporary relative density of a WIMP particle χ [8]:

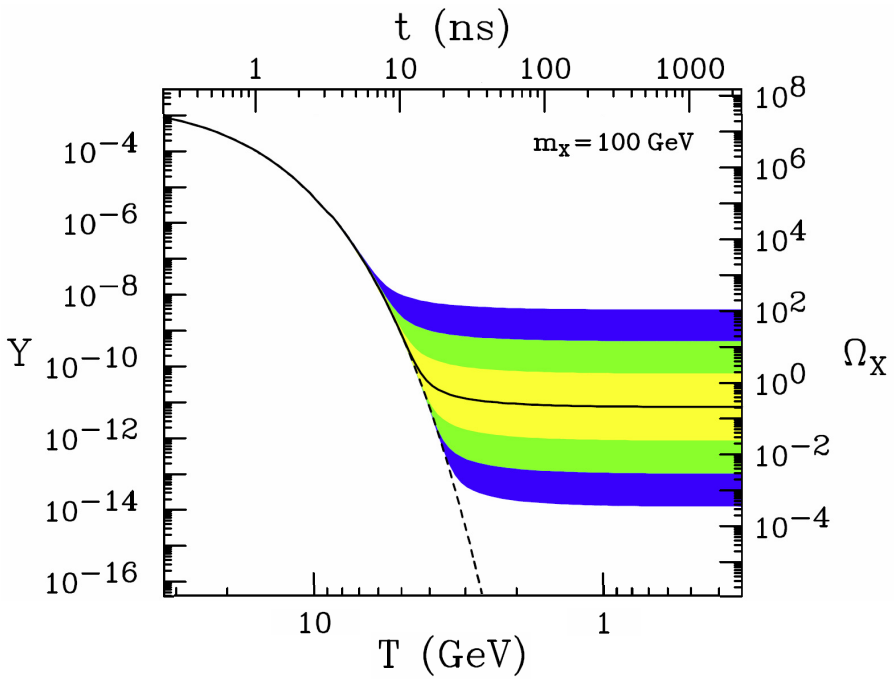

Figure 1.4: The evolution of the WIMP number density for a 100 GeV mass, as a function of temperature. The solid line corresponds to a freeze out temperature that gives the correct abundance for a dark matter candidate. The colored contours correspond to different freeze out temperatures, giving too high or too low abundance. From [16].

$$\begin{aligned}\Omega_\chi h^2 &= \frac{\rho h^2}{\rho_C} \\ &= \frac{m_\chi s_0 Y_0 h^2}{\rho_C} \\ &= 2.755 \times 10^8 \, Y_0 \, m_\chi \mathrm{GeV}^{-1}. \end{aligned} \tag{1.19}$$

To get the final numerical values, the present CMB temperature and a value of h_{eff} corresponding to photons and three neutrino species have been used.

The evolution of the (comoving) WIMP number density with decreasing temperature (increasing time) in the early Universe is shown in Figure 1.4. In the beginning it decreases very quickly and then after a some time freezes out, at which point it becomes constant. It is clear that the mass of the particle has an impact on when freeze-out happens, but perhaps more interestingly is the dependence of the relic density on the cross section. The smaller the cross section, the larger the relic density. Or more explicitly:

$$\Omega_\chi h^2 \propto \frac{1}{\langle \sigma_{\mathrm{ann}} v \rangle}.$$

As it turns out, using the value for the weak cross section yields exactly the correct relic density for a dark matter particle as given by modern cosmology. This fact is often referred to as the

'WIMP miracle' and is one of the main motivations for the WIMP as a dark matter candidate. The WIMP is often taken to be one of the new particles in Supersymmetry, and many of the experimental searches look for a dark matter particle with the properties such a particle would have. In particular, it is often taken to be the so-called Lightest Supersymmetric Particle, which would be stable given certain assumptions in some Supersymmetric models. One of the more popular of these choices is the lightest neutralino [8].

Axions. Because of the way they are produced, WIMPs are also referred to as thermal dark matter. This is because they are produced by interactions in a thermal plasma, where they are in equilibrium with SM particles as described above. Particles produced in other ways are called non-thermal. Among these, the axion is a prime candidate.

The axion is the pseudo Nambu-Goldstone boson associated with the spontaneous symmetry breaking of the so-called PQ-symmetry [46, 45, 67, 68], named after Peccei and Quinn. It is introduced in the theory of strong interactions, quantum chromodynamics (QCD), in order to resolve the strong CP (Charge Parity) problem. Briefly stated, the QCD-Lagrangian has a term of the form [8]:

$$\mathcal{L}_{\text{QCD}} = ... + \frac{\theta g^2}{32\pi^2} G^a_{\mu\nu} \tilde{G}^{a\mu\nu}. \tag{1.20}$$

Here $G^a_{\mu\nu}$ is the color field strength tensor, the tilde signifying its dual. This term does not contribute perturbatively, but has been shown [63] to have physical significance through non-perturbative instanton effects. From this, it can be demonstrated that the parameter $\bar{\theta}$ (which depends on θ) must be non-zero, causing CP-violation. The problem is the fact that CP violation has not been observed in QCD, giving an upper bound of $\bar{\theta} \lesssim 10^{-10}$ [26]. To explain why this parameter is so small, one introduces the axion field.

The axion has a small, but non-zero mass and is a (pseudo)scalar. Its couplings to SM particles are very weak, which makes it interesting as a dark matter candidate. There is only one unknown parameter for the axion, which can either be taken to be the scale of PQ-symmetry breaking, or equivalently its mass, which depends on the other inversely. Unfortunately, there is a very large range of allowed values as far as the Standard Model is concerned. There are constraints from astrophysics, cosmology and particle experiments, which constrains the mass as $\lesssim 10^{-2}$ eV [26]. To have the correct relic density for a dark matter candidate, the mass should also not be too small, though this is very model dependent and depends on assumptions made in cosmology. For example, this would depend on whether the PQ-transition took place before or after inflation.

The case for the axion then, is the low number of extra content it adds to the Standard Model, while simultaneously solving the strong CP-problem and being a dark matter candidate. However, it is also very hard to detect, because of the way it interacts. As a consequence, it is a less popular candidate than for example the WIMP as far as current experimental searches go.

Super-heavy dark matter. Dark matter may also be in the form of very heavy ($\sim 10^{13}$GeV) particles. These particles must be produced non-thermally, because their large mass would cause them to freeze-out too soon, leading to an abundance in excess of the required value.

The particles in this category can have various properties and can even be a form of very heavy, non-thermal WIMP (termed WIMPZILLAs). The main production mechanism for these particles is gravitationally in an expanding Universe, in particular towards the end of inflation. As previously discussed, the inflaton field will at some point lose energy and decay into other particles. If the inflaton decays into particles with masses on the order of the Hubble parameter at the end of inflation – 10^{13} GeV – these particles can be found to have the correct relic density [8].

To accommodate the requirements for dark matter, the super-heavy particles may be either stable or very long lived (comparable to the age of the Universe). In the latter case, they may also provide an explanation for high energy cosmic rays. If the super-heavy particles decay into (e.g.,) protons, then the protons will be found to have large amounts of energy. This energy is consistent with some of the high energy cosmic rays that have been detected, and so far unexplained by other means.

Kaluza-Klein particles. Finally, a more exotic candidate is the Kaluza-Klein particle, which is realized in certain models with extra dimensions. The Kaluza-Klein theory [27, 28] was originally developed by Kaluza and Klein in the 1920s as an attempt to unify General Relativity with Electromagnetism in 5 dimensions. It did not see much use in its time, but was picked up again with the rise of string theory and other higher dimensional theories in the latter half of the century. The idea of the modern formulation is that of multiple compactified dimensions, in addition to the four regular ones. Within this framework arises an explanation for why gravity is so weak: it spreads out into these other dimensions and becomes suppressed.

Dark matter in this context can be excitations of SM fields in the compactified dimensions, the size of which depends on the model. These excitations, called Kaluza-Klein towers, appear as increased effective masses in our 4D world. The usual properties of dark matter candidates, like either stability or long life-times and sensible masses, apply also for the Kaluza-Klein particles. However, as with many other theories in the category of extra dimensions, the testability and experimental framework is somewhat elusive. Unless some evidence of extra dimensions are found at the LHC, the case for Kaluza-Klein models as a promising avenue of dark matter searches may be hard to make.

Final thoughts

In this chapter the basic equations, parameters, definitions and assumptions of cosmology and dark matter theory have been established. The Universe evolved from an initial singularity into its present state. This state is isotropic and homogeneous, with a flat geometry. The dynamic properties of the Universe are modeled by a metric. This metric is a solution to the Einstein equation for a given energy-momentum tensor. This leads to equations for the scale factor, which describes the time evolution of the spatial component of the Universe. It also motivates the definition of the Hubble parameter, which, being derived from the scale factor, often appears in cosmological equations to account for the properties of the expansion of the Universe. There are certain problems with the resulting model, but these can be resolved if, at very early times, the Universe underwent a period of rapid expansion called inflation. The Universe as defined by

the ΛCDM model contains mostly dark matter and a cosmological constant. Dark matter is a so far undiscovered type of matter which does not interact with photons. The existence of dark matter is proposed due to its observed gravitational effects, as well as the fact that the measured matter content of the Universe can not be accounted for by ordinary matter. There are several candidates for the particle nature of dark matter, but the most favored currently is the WIMP. The properties of the WIMP give the correct relic density, and allow for interactions that make it detectable in specific experiments. The WIMP is often modeled as a supersymmetric particle.

As far as the rest of the thesis goes, the important parts of the above to keep in mind are: The Hubble parameter, which appears in equations that are affected by the expansion of the Universe, e.g., integrals over redshift. The assumption of isotropy and homogeneity, which will be needed in calculations. In particular when using average values for the distributions of galaxies, and when taking the total synchrotron intensity to be isotropic. Finally, the properties of WIMPs, which will be important when motivating the main goal of the thesis. Specifically, why synchrotron radiation from cosmic rays is a viable alternative compared to synchrotron radiation with a dark matter origin.

Chapter 2:

The extra-galactic radio background

In addition to all sources in the Universe that can be resolved with telescopes and satellites, there are unresolved ones that contribute to the background radiation only. The most famous example of this is the CMB, but there is also a radio background. In particular, there is an extra-galactic radio background consisting of radio waves from galaxies and clusters all over the Universe. The origins of this radiation are manifold, and a few of them will be explored later. The section begins with the theoretical framework of one type of radiation contributing to the radio background, namely synchrotron radiation.

2.1 Synchrotron radiation

A fundamental concept of physics, is that of charged particles emitting electromagnetic radiation when they are accelerated. In many cases this is caused by application of an electric field, which by the Lorentz force law:

$$\mathbf{F} = q\mathbf{E} + q\mathbf{v} \times \mathbf{B},$$

causes collinear (with respect to the field) acceleration proportional to the field strength. However, in the interstellar regions of the galaxy there are no large scale electric fields, only magnetic fields. As is evident from the Lorentz force law, the acceleration of a charged particle by a magnetic field is always perpendicular to the velocity of the particle. Hence, in the presence of galactic magnetic fields, electrons will undergo helical motion. The radiation produced by this type of acceleration is called cyclotron radiation, or for particles with ultra-relativistic speeds, synchrotron radiation.

2.1.1 The synchrotron power of a single particle

The Liénard-Wiechert potentials [25, 36] are given by:

$$\mathbf{A}(\mathbf{r},t) = \frac{\mu_0}{4\pi r}\left[\frac{q\mathbf{v}}{1-\boldsymbol{\beta}\cdot\mathbf{n}}\right]_{\text{ret}}, \tag{2.1}$$

$$\phi(\mathbf{r},t) = \frac{1}{4\pi\epsilon_0 r}\left[\frac{q}{1-\boldsymbol{\beta}\cdot\mathbf{n}}\right]_{\text{ret}}, \tag{2.2}$$

where $\mathbf{v}$ is the particle velocity, $\boldsymbol{\beta} \equiv \mathbf{v}/c$, $\mathbf{n}$ is the normal vector in the direction from the observer to the source and 'ret' indicates that the expression is to be evaluated at the retarded time.

The total energy radiated per unit solid angle is [25]:

$$\frac{\mathrm{d}W}{\mathrm{d}\Omega} = \int_{-\infty}^{\infty} \mathrm{d}t\, |\mathbf{A}(t)|^2.$$

Using the Fourier transform of $\mathbf{A}$ and the inverse transform:

$$\mathbf{A}(\omega) = \frac{1}{\sqrt{2\pi}}\int_{-\infty}^{\infty} \mathrm{d}t\, \mathbf{A}(t)\, \mathrm{e}^{\mathrm{i}\omega t}, \tag{2.3}$$

$$\mathbf{A}(t) = \frac{1}{\sqrt{2\pi}}\int_{-\infty}^{\infty} \mathrm{d}\omega\, \mathbf{A}(\omega)\, \mathrm{e}^{-\mathrm{i}\omega t}, \tag{2.4}$$

it is trivial to see that:

$$\frac{\mathrm{d}W}{\mathrm{d}\Omega} = \int_{-\infty}^{\infty} \mathrm{d}\omega\, |\mathbf{A}(\omega)|^2.$$

The unphysical nature of negative frequencies motivates writing the above as:

$$\frac{\mathrm{d}W}{\mathrm{d}\Omega} = \int_{0}^{\infty} \mathrm{d}\omega \left(|\mathbf{A}(\omega)|^{\,2} + |\mathbf{A}(-\omega)|^{\,2} \right).$$

This leads to an expression for the energy radiated per unit solid angle per unit frequency:

$$\frac{\mathrm{d}^2 I}{\mathrm{d}\omega\, \mathrm{d}\Omega} = |\mathbf{A}(\omega)|^2 + |\mathbf{A}(-\omega)|^2,$$

which by (2.3) is easily seen to be:

$$\frac{\mathrm{d}^2 I}{\mathrm{d}\omega\, \mathrm{d}\Omega} = |\mathbf{A}(\omega)|^2 + |\mathbf{A}^*(\omega)|^2,$$

$$\frac{\mathrm{d}^2 I}{\mathrm{d}\omega\, \mathrm{d}\Omega} = 2\,|\mathbf{A}(\omega)|^2. \tag{2.5}$$

Using $\kappa \equiv 1 - \boldsymbol{\beta} \cdot \mathbf{n}$, as well as (2.1), (2.3) and (2.5) we get [36]:

$$\frac{\mathrm{d}^2 I}{\mathrm{d}\omega\, \mathrm{d}\Omega} = \frac{\mathrm{q}^2}{16\pi^3 \epsilon_0 c} \left| \int_{-\infty}^{\infty} \mathrm{d}t \left\{ \mathbf{n} \times \left[(\mathbf{n} - \boldsymbol{\beta}) \times \dot{\boldsymbol{\beta}} \right] \kappa^{-3} \right\}_{\mathrm{ret}} \mathrm{e}^{\mathrm{i}\omega t} \right|^2 . \tag{2.6}$$

Utilizing that:

$$\mathbf{n} \times ((\mathbf{n} - \boldsymbol{\beta}) \times \dot{\boldsymbol{\beta}}) \kappa^{-2} = \frac{\mathrm{d}}{\mathrm{d}t'} (\kappa^{-1} \mathbf{n} \times (\mathbf{n} \times \boldsymbol{\beta})),$$

where t′ is the retarded time, making a substitution to t′ in (2.6) and doing a partial integration gives:

$$\frac{\mathrm{d}^2 I}{\mathrm{d}\omega\, \mathrm{d}\Omega} = \frac{\mathrm{q}^2 \omega^2}{16\pi^3 \epsilon_0 c} \left| \int_{-\infty}^{\infty} \mathrm{d}t' \mathbf{n} \times (\mathbf{n} \times \boldsymbol{\beta}) \exp\left[\mathrm{i}\omega \left(t' - \frac{\mathbf{n} \cdot \mathbf{r}_0(t')}{c} \right) \right] \right|^2 .$$

Here, $\mathbf{r}_0$ is the position vector of the particle with respect to the origin.

Following [36] one can introduce a coordinate system for describing the polarization of the radiation, $\boldsymbol{\epsilon}_\perp$ and $\boldsymbol{\epsilon}_\parallel$, representing the directions perpendicular and parallel to the magnetic field respectively, with the property that $\boldsymbol{\epsilon}_\parallel = \mathbf{n} \times \boldsymbol{\epsilon}_\perp$. Then, making use of natural approximations valid for ultra-relativistic velocities, one obtains (after some algebra):

$$\frac{\mathrm{d}^2 I_\perp(\omega)}{\mathrm{d}\omega\, \mathrm{d}\Omega} = \frac{\mathrm{q}^2 \omega^2}{16\pi^3 \epsilon_0 c} \left| \int_{-\infty}^{\infty} \mathrm{d}t' \frac{v t'}{a} \exp\left[\frac{\mathrm{i}\omega}{2\gamma^2} \left(t'(1 + \gamma^2 \theta^2) + \frac{c^2 \gamma^2}{3a^2} t'^3 \right) \right] \right|^2 , \tag{2.7}$$

$$\frac{\mathrm{d}^2 I_\parallel(\omega)}{\mathrm{d}\omega\, \mathrm{d}\Omega} = \frac{\mathrm{q}^2 \omega^2 \theta^2}{16\pi^3 \epsilon_0 c} \left| \int_{-\infty}^{\infty} \mathrm{d}t' \exp\left[\frac{\mathrm{i}\omega}{2\gamma^2} \left(t'(1 + \gamma^2 \theta^2) + \frac{c^2 \gamma^2}{3a^2} t'^3 \right) \right] \right|^2 . \tag{2.8}$$

Here we have γ as the usual Lorentz factor, θ as the angle between the x-y plane (where the circular motion takes place) and $\mathbf{n}$, and a as the radius of curvature (relativistic Larmor radius) of the orbit.

Making some further variable substitutions, using standard formulas for the integrals and finally integrating over the solid angle, (2.7) and (2.8) become:

$$I_\perp(\omega) = \frac{\sqrt{3} \mathrm{e}^2 \gamma \sin\alpha}{8\pi \epsilon_0 c} \left[x \int_x^{\infty} \mathrm{d}y\, K_{5/3}(y) + x K_{2/3}(x) \right], \tag{2.9}$$

$$I_\parallel(\omega) = \frac{\sqrt{3} \mathrm{e}^2 \gamma \sin\alpha}{8\pi \epsilon_0 c} \left[x \int_x^{\infty} \mathrm{d}y\, K_{5/3}(y) - x K_{2/3}(x) \right]. \tag{2.10}$$

In the above expressions, α is the pitch angle (the angle between the velocity and the magnetic field), $x \equiv 2\omega a/(3c\gamma^3)$, while $K_{5/3}$ and $K_{2/3}$ are the modified Bessel functions of order $5/3$ and $2/3$ respectively. Defining the critical angular frequency by $\omega_c \equiv 3c\gamma^3/(2a)$ we get:

$$x = \frac{\omega}{\omega_c} = \frac{\nu}{\nu_c}.$$

The critical frequency can be rewritten by using that $a = v\gamma m/(\mathrm{e}B\sin\alpha)$ (B being the magnetic field strength). In the ultra-relativistic limit, the critical frequency consequently takes the form:

$$\nu_c = \frac{3}{2}\frac{\mathrm{e}B}{2\pi m}\gamma^2 \sin\alpha. \tag{2.11}$$

Dividing (2.9) and (2.10) by the orbital period $T_{\mathrm{orbit}} = 2\pi\gamma m/(\mathrm{e}B)$ yields the power per unit frequency for the two polarizations:

$$W_\perp = \frac{I_\perp}{T_{\mathrm{orbit}}} = \frac{\sqrt{3}\mathrm{e}^2 B\sin\alpha}{16\pi^2\epsilon_0 mc}\left[x\int_x^\infty \mathrm{d}y\, K_{5/3}(y) + xK_{2/3}(x)\right],$$
$$W_\parallel = \frac{I_\parallel}{T_{\mathrm{orbit}}} = \frac{\sqrt{3}\mathrm{e}^2 B\sin\alpha}{16\pi^2\epsilon_0 mc}\left[x\int_x^\infty \mathrm{d}y\, K_{5/3}(y) - xK_{2/3}(x)\right].$$

Finally, we obtain the total synchrotron power per unit frequency for a single particle by adding the two above expressions and changing from angular frequency to frequency by multiplication of 2π:

$$P_s(\nu,\gamma,\alpha) = \frac{\sqrt{3}e^3 B\sin\alpha}{4\pi\epsilon_0 mc}F(\nu/\nu_c), \tag{2.12}$$

where F is:

$$F(\nu/\nu_c) \equiv \frac{\nu}{\nu_c}\int_{\nu/\nu_c}^\infty \mathrm{d}y\, K_{5/3}(y). \tag{2.13}$$

The behavior of the Bessel integral is that of a power law for $\nu \ll \nu_c$. For $\nu \gg \nu_c$ it is exponentially decaying. Most of the power is radiated at a frequency $\nu \approx 0.29\nu_c$. This is shown in Figure 2.1.

2.1.2 Synchrotron intensity

To find the intensity per unit frequency from a population of electrons, we first need the emissivity and the absorption coefficient. The synchrotron emissivity is given by:

$$\epsilon_\nu(\nu,\alpha) = \int_{\gamma_1}^{\gamma_2} \mathrm{d}\gamma\, N(\gamma)P_s(\gamma,\nu,\alpha) \tag{2.14}$$

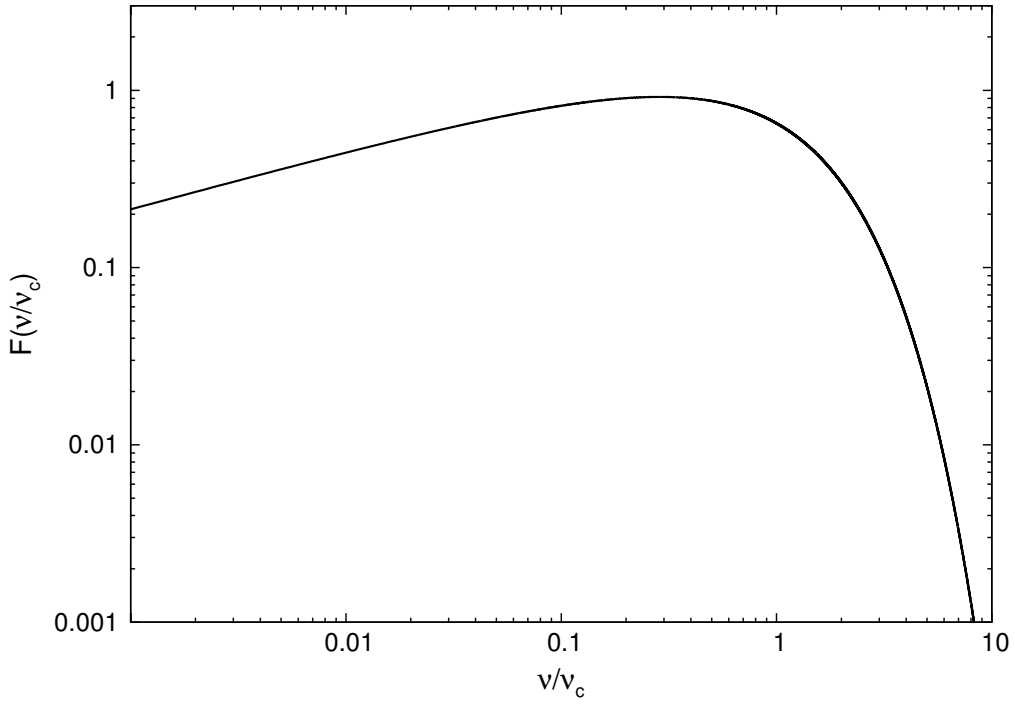

Figure 2.1: The Bessel integral from (2.13), showing the behavior around the critical frequency.

where $N(\gamma)$ is the number density of electrons as a function of the Lorentz factor. The integral is over the range of realistic values of γ for the situation of interest. In theory these could be one and infinity, but for most cases (like e.g. a power law) there will be a low and high energy cutoff.

The absorption coefficient can be found by considering an electron in a 2-level system, and the spontaneous emission of a photon during a transition from level 2 to level 1 (decreasing the energy and momentum). The synchrotron power can then be expressed through the Einstein coefficient for spontaneous emission:

$$P_{\mathrm{s}} = h\nu A_{21},$$

where ν is the frequency of the emitted photon. The corresponding coefficients for stimulated emission and absorption, B_{21} and B_{12} respectively, are equal to each other and related to A_{21} in the following way:

$$A_{21} = \frac{2h\nu^3}{c^2} B_{12}.$$

A transition from 2 to 1 is a transition from E to $E - \mathrm{d}E$ and p to $p - \mathrm{d}p$. Furthermore, the Einstein coefficients are defined in terms of the number density of electrons per phase space

volume $\mathrm{d}^3\mathbf{p}$, $n(\mathbf{p})$. The two states are then separated by $\mathrm{d}\mathbf{p} = \hbar\mathbf{k}$. The absorption coefficient for this process follows as:

$$\kappa'_\nu = \frac{h\nu}{4\pi}\left[n(\mathbf{p}-\hbar\mathbf{k})B_{12}\mathrm{d}^3\mathbf{p} - n(\mathbf{p})B_{21}\mathrm{d}^3\mathbf{p}\right].$$

Since the momentum difference should be small, one can expand the number density to first order and get:

$$n(\mathbf{p}-\hbar\mathbf{k}) = n(\mathbf{p}) - \frac{h\nu}{c}\frac{\mathrm{d}n}{\mathrm{d}p},$$

where the absolute value of $\mathbf{k}$ is $2\pi\nu/c$. This then gives:

$$\kappa'_\nu = -\frac{h^2\nu^2}{4\pi c}\frac{\mathrm{d}n}{\mathrm{d}p}B_{12}.$$

Taking the integral of the above expression over all possible momentum states, gives the total synchrotron absorption coefficient:

$$\kappa_\nu = -\frac{h^2\nu^2}{4\pi c}\int_0^\infty \mathrm{d}p\,\frac{\mathrm{d}n}{\mathrm{d}p}\,B_{12}\,4\pi p^2,$$

where it was assumed that the distribution is isotropic in momentum space. Inserting the expression for B_{12} yields:

$$\kappa_\nu = -\frac{c}{2\nu^2}\int_0^\infty \mathrm{d}p\,P_\mathrm{s}(\nu,p)\frac{\mathrm{d}n}{\mathrm{d}p}\,p^2.$$

Changing variables to energy and noting that, since the electron is ultra-relativistic, $E = pc$, and also that:

$$4\pi p^2 n(p)\mathrm{d}p = N(E)\mathrm{d}E,$$

yields:

$$\kappa_\nu = -\frac{c^2}{8\pi\nu^2}\int_0^\infty \mathrm{d}E\,P_\mathrm{s}(\nu,E)E^2\frac{\mathrm{d}}{\mathrm{d}E}\left(\frac{1}{E^2}N(E)\right).$$

Making use of the fact that the two factors (without the differential operator) together evaluate to zero on the boundary, a partial integration gives:

$$\kappa_\nu = \frac{c^2}{8\pi\nu^2}\int_0^\infty \mathrm{d}E\,\frac{1}{E^2}N(E)\frac{\mathrm{d}}{\mathrm{d}E}\left(P_\mathrm{s}(\nu,E)E^2\right).$$

A final change of variables to the Lorentz factor gives the desired result:

$$\kappa_\nu(\nu,\alpha) = \frac{1}{8\pi m\nu^2}\int_{\gamma_1}^{\gamma_2}\mathrm{d}\gamma\,\frac{N(\gamma)}{\gamma^2}\frac{\mathrm{d}}{\mathrm{d}\gamma}\left[\gamma^2 P_s(\gamma,\nu,\alpha)\right], \tag{2.15}$$

where everything is as for the emissivity. For an isotropic distribution of pitch angles, both (2.14) and (2.15) must be averaged.

To get the emitted intensity just outside the source, one must in general solve a transport equation. The decrease in intensity when moving a distance $\mathrm{d}x$ is $k_\nu I_\nu\,\mathrm{d}x$. Similarly, the increase in intensity is $\epsilon_\nu\,\mathrm{d}x/4\pi$. This gives:

$$\frac{\mathrm{d}I_\nu}{\mathrm{d}x} = \frac{\epsilon_\nu}{4\pi} - k_\nu S_\nu$$

For a region of optical thickness R, the solution to this equation is [36]:

$$I_\nu = \frac{\epsilon_\nu}{4\pi\kappa_\nu}(1-\mathrm{e}^{-\tau_\nu})$$

where $\tau_\nu \equiv \kappa_\nu R$ is the optical absorption depth. If there is very little absorption, $\tau_\nu \ll 1$, the exponential can be expanded to yield:

$$I_\nu = \frac{\epsilon_\nu R}{4\pi}. \tag{2.16}$$

If there is much absorption, $\tau_\nu \gg 1$, the exponential term disappears. This gives:

$$I_\nu = \frac{\epsilon_\nu}{4\pi\kappa_\nu}. \tag{2.17}$$

If $N(\gamma)$ is a power law, this can be shown [36] to be simply:

$$I_\nu \propto \nu^{5/2}.$$

This thesis is concerned with the case where absorption can be neglected. Combining (2.12), (2.14) and (2.16) then gives:

$$I_\nu = \frac{R}{4\pi}\left\langle\int_{\gamma_1}^{\gamma_2}\mathrm{d}\gamma\,N(\gamma)\frac{\sqrt{3}e^3 B\sin\alpha}{4\pi\epsilon_0 m_e c}F(\nu/\nu_c)\right\rangle, \tag{2.18}$$

where the brackets indicate averaging over the angular distribution. For a power law distribution of the form $N(\gamma) \propto \gamma^{-p}$, the angular dependence will be of the form $\sin^{(p+1)/2}(\alpha)$. The angular average is then:

$$\frac{1}{2}\int_0^\pi \mathrm{d}\alpha\ \sin^{(p+3)/2}(\alpha) = \frac{\sqrt{\pi}}{2}\frac{\Gamma\left(\frac{(p+5)}{4}\right)}{\Gamma\left(\frac{(p+7)}{4}\right)}.$$

This will simply be a factor of order 1.

In general, (2.18) is the final expression for the synchrotron intensity from a distribution of electrons in a regime with little to no absorption. In particular, it is the intensity per unit frequency just outside the source. This can be used to yield the synchrotron luminosity per unit frequency of a galaxy, where the cosmic ray electrons have a particle spectrum given by $N(\gamma)$. This will be discussed in detail later.

An important parameter in this setting is the spectral index of the intensity (or luminosity), defined as the negative power of the frequency dependence for a power law spectrum:

$$I_\nu \propto \nu^{-\alpha} \tag{2.19}$$

For electrons following a power law, a simple relation between the electron power dependence – $N(\gamma) \propto \gamma^{-p}$ – and the spectral index of the intensity of the corresponding synchrotron radiation can be found. Since most of the radiation is emitted at $0.29\,\nu_c$, assuming that all of the radiation is emitted at this frequency is a fair approximation. Then the emissivity at a frequency $\nu = 0.29\,\nu_c \propto \gamma^2$, within the interval $\mathrm{d}\nu$, comes from electrons with an energy γ, in the interval $\mathrm{d}\gamma$. In other words:

$$\begin{aligned}\epsilon_\nu\,\mathrm{d}\nu &= \frac{1}{4\pi}P_s N(\gamma)\,\mathrm{d}\gamma,\\ \epsilon_\nu &\propto \left(\gamma^2\gamma^{-p}\right)\frac{\mathrm{d}\gamma}{\mathrm{d}\nu}.\end{aligned}$$

Thus the frequency dependence is:

$$\begin{aligned}\epsilon_\nu &\propto \nu^{(2-p)/2}\,\nu^{-1/2},\\ &\propto \nu^{-(p-1)/2}.\end{aligned}$$

From the above, (2.16) and (2.19), the relation between the spectral index and the electron power dependence follows as $\alpha = (p-1)/2$.

2.2 Cosmic Rays

Stated simply, cosmic rays are high energy particles propagating through the Universe. They have kinetic energies ranging from roughly 10^7 eV to 10^{20} for the ultra-high energy cosmic rays [57]. Most cosmic rays are protons or atomic nuclei (98%), but there are also electrons (2%). They are mostly detected by their collisions with the upper atmosphere, and it was through this mechanism that they were first discovered in 1912 by Victor Hess in a balloon experiment. Superficially they are important due to this interaction and its effect on the Earth, but in general they can reveal much about our own galaxy, for example the properties of the interstellar medium and the galactic magnetic fields. They can also elucidate certain properties of extra-galactic space, for example the nature of active galaxies and extra-galactic magnetic fields.

2.2.1 Origin

The origin of cosmic rays has long been believed to be supernova remnants [36]. Specifically, the particles are trapped and accelerated by magnetic fields in the interstellar gas, through which shock waves from the supernova explosion move. The high amount of acceleration comes from repeated movement across the shock front. In general, the motion is a diffusive random walk through the interstellar medium, and the particles will escape eventually. The first formulation of this theory was by Fermi [17], but his model did not involve supernovae and had other weaknesses as well. This was expanded later to the diffusive shock acceleration model by several authors working independently [3, 7, 10, 32]. In practice, this is a quite complex process, and much effort has gone into computer simulations. The main success of the model is its ability to produce the desired power law spectrum that cosmic rays are observed to have, as well as predict their high energies.

However, there is a maximum value for the energy that can be attained this way. Thus, it is not possible to account for the full energy spectrum of cosmic rays in this manner. In other words, the origin of ultra-high energy cosmic rays remains unknown. The main candidates are active galactic nuclei (AGN) [57]. They are centers of galaxies with a particularly strong signal, of non-thermal origin, in some or all of the electromagnetic spectrum. This is believed to be due to accretion of matter by the central super-massive black hole. Such accretion could also accelerate particles to the observed energies of the ultra-high energy cosmic rays. Another candidate for the production of ultra-high energy cosmic rays is the decay of very heavy particles, possibly dark matter if it indeed is in such a form. Such annihilation would be expected to produce the stable SM particles like electrons, protons, photons and neutrinos and could therefore produce cosmic rays. In particular, because they are so heavy, they could also produce cosmic rays with high enough energies. Generally, the production mechanism for ultra-high energy cosmic rays depends on the species, that is whether they are protons or light nuclei. Clearly, one would not expect nuclei to be produced in annihilations, but they could be accelerated by AGN.

2.2.2 Propagation

Cosmic rays produced in our galaxy, say by supernova remnants, will be scattered by interactions with the interstellar medium [60]. This is sometimes in the form of collisions with interstellar matter, which also produce secondary particles, but the dominant contribution is from deflections by galactic magnetic fields. The field strength and direction of these fields vary somewhat with location in the galaxy. The net effect of both of these contributions is some energy loss, as well as the isotropization of arrival directions. The latter being a problem for experimental verification of the production mechanism, as the cosmic rays can not be directly traced back to any supernova remnant. Since synchrotron radiation from electrons is the main subject of this thesis, only diffusion by magnetic fields will be discussed in detail.

The precise nature of the galactic magnetic field is not known with a high degree of certainty. It is difficult to measure the large scale structure from within the Milky Way. Hence, much of the current theory is based on observations of other galaxies. The total field is modeled as a regular field which follows the distribution of matter, i.e., as a spiral disk (too little is known about the magnetic field inside the bulge). This can be either axisymmetric or bisymmetric, meaning a symmetry with respect to a rotation of 2π or π respectively. While the former cannot be excluded, the bisymmetric model (see Figure 2.2) is currently best supported by evidence [60]. In this model, the field strength is given by:

$$B(r, \theta) = B_0(r) \cos\left(\theta - \delta \ln(r/r_0)\right).$$

Here r and θ are the usual polar coordinates, r_0 is the distance from the galactic center where the maximum field strength is attained (10.55 kpc) and $\delta = \tan(\alpha^{-1})$. α being the angle between the spiral and the galactic plane. The field strength is assumed to be exponentially suppressed above and below the disk. $B_0(r)$ could for instance be defined to be about 2 μG at the position of the solar system and to be inversely proportional to the distance at 4 kpc or more. There is also a halo component with different structure that needs to be considered. This could for instance be a toroidal dipole field that decreases as r^{-3}. Additionally there are turbulent components of the field that need to be treated with special care.

The motion of the cosmic rays are determined by letting the particles diffuse in the magnetic field. Although there are large fluctuations in the field, it is possible to study this motion, as one usually is interested in large scale, and therefore average, behavior. Diffusion is given in terms of the time evolution of the number density of the particle. It is thus important to consider the energy losses induced by the interactions with the interstellar medium. For electrons, the dominant energy loss is through interactions with the magnetic field, i.e., synchrotron radiation, and inverse Compton scattering with the CMB. A diffusion-loss equation for the number density can then be given by considering the energy loss, combined with the injection of new particles from sources in the galaxy. Such an equation is typically written like [36]:

$$\frac{\mathrm{d}N(E)}{\mathrm{d}t} = D\nabla^2 N(E) + \frac{\partial}{\partial E}\Big(b(E)N(E)\Big) + Q(E), \tag{2.20}$$

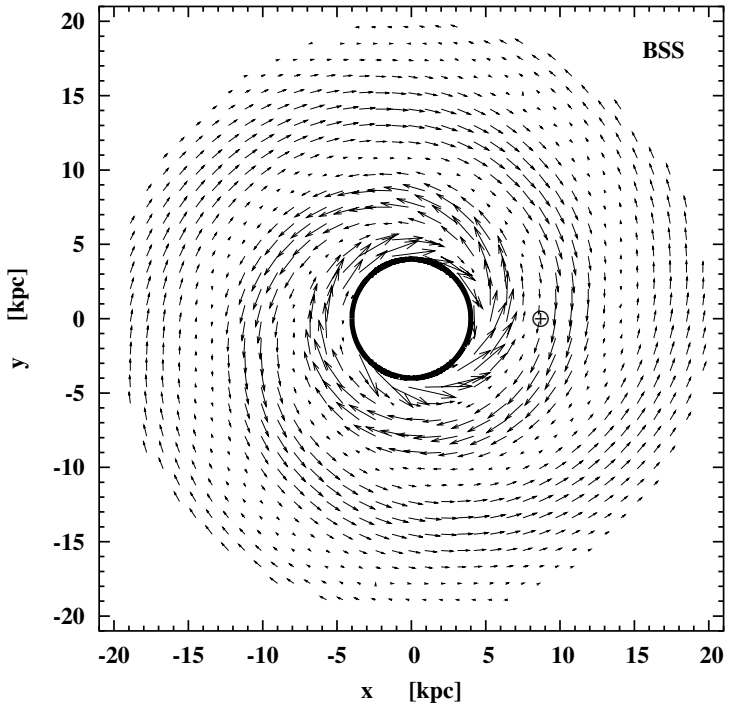

Figure 2.2: The bisymmetric model for the magnetic field in the disk of the Milky Way, the position of the Sun is marked. Taken from [2].

where D is the diffusion coefficient, b is the energy loss and Q is the source term.

A much used model for the diffusion of cosmic rays is the 'leaky box' model. In this framework, the galaxy is considered as a box with a certain volume, inside which cosmic rays are produced by sources and move around (diffuse). At any given time there is a certain probability for a cosmic ray to escape the galaxy (leak outside the box). The important parameter is the mean distance traveled by the cosmic rays before they escape, or, equivalently, the lifetime of the particle in the galaxy, τ. In this model the diffusion term in (2.20) becomes $N(E)/\tau(E)$.

At energies on the order of 10^{15}eV there is a change of slope in the energy spectrum power law, called 'the knee'. This is a steepening of the spectrum, i.e., the number of cosmic rays at a given energy decreases faster above this value, see Figure 2.3 for details. The cause of this is most likely a change in the diffusion coefficient. This comes from the fact that higher energy particles are more likely to escape the galaxy. In particular, there should be a point where this starts to change more abruptly, as the magnetic field becomes unable to contain the cosmic rays the way it does for lower energies. For an electron at 10^{15}eV in a magnetic field $\sim$ μG, the Larmor radius is roughly of order 1 pc. Comparing with the thickness of the disk, 300 pc, the chance that a particle will escape is clearly non-trivial. Another explanation might be a lack of sources above this energy, but if the supernova origin is correct (as seems likely at this point), one would expect the cutoff energy to be larger than the previously mentioned value.

As discussed earlier, the origin of the most energetic cosmic rays are extra-galactic. Consequently, their propagation is to a larger extent a journey from A to B than a random walk. Though they are somewhat deflected by both galactic and extra-galactic magnetic fields, their energies are too high (and the magnetic fields too weak) for this to be more than a slight deflection. As a

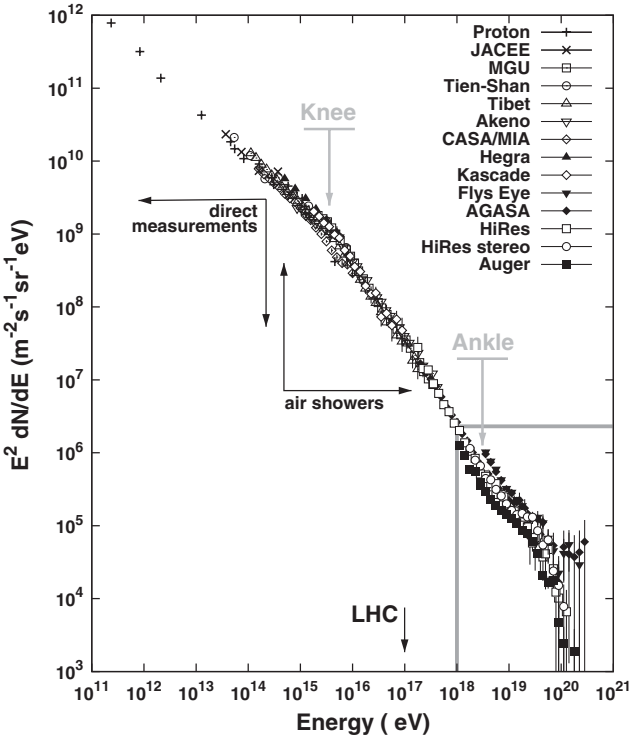

Figure 2.3: Plot of the high energy part of the cosmic ray spectrum, showing some of the steep slope and some of the experimental details. Taken from [33].

consequence, there is a higher degree of anisotropy (though it is still quite small), especially at the highest energies, which makes it easier to guess the direction from which the cosmic rays originate. Additionally, if the cosmic rays are produced by AGN, they should not arrive from all directions, but only from regions where AGN are known to be located. The most important interaction for ultra-high energy cosmic rays are with the CMB. The most notable effect of this interaction being the Greisen-Zatsepin-Kuz'min (GZK) cutoff [22, 69]. When the energy of cosmic ray protons is high enough, photo-pion and photo-pair production will occur. In particular, the relevant reactions are [36]:

$$\gamma + \mathrm{p} \rightarrow \mathrm{n} + \pi^{+},$$
$$\gamma + \mathrm{p} \rightarrow \mathrm{p} + \pi^{0} \rightarrow \mathrm{p} + 2\gamma,$$
$$\gamma + \mathrm{p} \rightarrow \mathrm{p} + N\pi.$$

These reactions deplete the cosmic ray energy, leading to a cutoff at 5×10^{19}eV if the protons propagate long enough. However, protons with these energies have been detected. The interpretation of this observation is that the sources for these protons must be within a distance of 30 Mpc, in other words, within the cosmic neighborhood of our galaxy. Another reaction that has an influence on the cosmic ray spectrum is electron-positron production. Because of the lower mass of the electron, this process does not deplete as much energy as the production of pions. The effect is therefore less noticeable on the highest energy particles, but it does influence the spectrum down to energies of roughly 10^{18}eV, which is the threshold energy for this process. Cosmic ray nuclei will also have a high energy cutoff, in this case due to photo-nuclear disintegration. This is the process where the nucleus is excited by photons, which in turn leads to the escape of one or more nucleons. The energies relevant here are on the order

of the GZK cutoff.

2.3 The radio background

Radio waves are photons with frequencies within the radio waveband. The exact definition of this waveband varies, but the upper limit is usually taken to be at 1 THz or less. For astronomy, there is also a lower limit in terms of what can be observed at Earth, due to the ionosphere, which is roughly at the order of 1 MHz. Radio sources can be galactic or extra-galactic, and the sources range from compact objects like pulsars to gas clouds and synchrotron radiation from cosmic rays. While galactic sources can often be resolved with high-resolution instruments, extra-galactic ones often can not. In particular, only very powerful galaxies (AGN) or ones in our neighborhood can be resolved clearly, while the rest only contribute to what is called the (diffuse) extra-galactic radio background of unresolved sources. This radiation can be further subdivided into thermal and non-thermal parts.

2.3.1 Thermal radiation

For the most part, thermal radiation is taken to be black-body radiation, hence the spectrum follows the famous Planck law:

$$I_\nu(\nu, T) = \frac{2h\nu^3}{c^2}\left[\exp\left(\frac{h\nu}{k_B T_b}\right) - 1\right]^{-1}, \tag{2.21}$$

where I_ν is the intensity per unit frequency per unit solid angle, h is the Planck constant, k_B the Boltzmann constant and T the temperature. Though there are few true black-body sources, it is a valid approximation for many cases. The Planck law is often used to model starlight and the thermal radiation of planets, and provides a very good fit to the spectrum of the CMB. For low frequencies and/or high temperatures, $h\nu \ll k_B T$, the exponential term is small and can be expanded to first order to obtain the Rayleigh-Jeans law:

$$I_\nu(\nu, T) = \frac{2k_B T\nu^2}{c^2}. \tag{2.22}$$

This is a characteristic power law in frequency which is often encountered in astrophysical spectra.

Radiation that is referred to as thermal is produced in systems where energy is transferred between particles and atoms or molecules, rather than say charged particles radiating in magnetic fields. These systems are gas clouds and plasmas where collisions, and hence thermal excitations, occur. It is important to separate between continuous emissions and line emissions. The most important contribution in the latter category is from what is known as the 21 cm line of neutral hydrogen, referring to the wavelength emitted (corresponding to a frequency of about 1.4 GHz).

The 21 cm line is an emission corresponding to the hyperfine splitting of the energy levels of the 1S ground state. This emission line is quite distinct, and its properties are well known theoretically. Hence, it is very useful for gathering information about the ambient locations. In particular, it is well suited for studying Doppler shifts and hence rotational velocities in galaxies and clusters. The transition corresponding to this emission is actually very rare, but due to the large amounts of hydrogen present in the Universe, it gives a visible contribution to the total thermal radiation flux. Continuous thermal emission is often in the form of black-body radiation, or near black-body radiation (gray-body radiation), as discussed in the previous paragraph.

2.3.2 Non-thermal radiation

The most significant contribution to non-thermal radiation in the radio waveband comes from synchrotron radiation. As has been noted previously, synchrotron radiation is produced by ultra-relativistic charged particles in magnetic fields. While there are many scenarios where synchrotron radiation is produced, the ones of interest for radio frequencies are cosmic rays diffusing in galactic magnetic fields. In particular, the main contribution comes from electrons rather than protons. This is because the critical frequency (see (2.11)) depends on the mass of the particle and its Lorentz factor, and the much heavier protons will at similar total energies emit radiation at much lower frequencies than corresponding electrons. The production and propagation of cosmic ray electrons result in a power law distribution in energy for any galactic population of said type. This in turns yields a synchrotron spectrum, which has a power law form until the maximum particle energy leads to an exponential cutoff in the spectrum.

Other dominant features of the synchrotron spectrum are that below a certain frequency, roughly at 1 MHz, synchrotron self-absorption losses become important. That is, the emitting electron distributions absorb large amounts of the radiation before it can escape. This yields a power law as given by (2.17). Additionally, observations of the synchrotron intensity of the Milky Way have suggested that the electron distribution might in fact be a broken power law, with a break at a few GeV [66]. This likely stems from a corresponding break in the diffusion coefficient, similar to the case of the 'knee'. If this is indeed the case for most or all normal spiral galaxies, it will have a visible effect on the extra-galactic synchrotron spectrum, causing a corresponding break in the spectral index. However, the break will be somewhat smoothed out. This is caused by the fact that there is not a strict one-to-one correspondence between particle energy and emission frequency, even though there is a dominant contribution from one energy value per frequency.

Typically, synchrotron radiation is dominant at lower frequencies, while thermal emission dominates at higher frequencies. Furthermore, they tend to have different shapes, thermal radiation being flatter (spectral index closer to 0). In general however, it is not straightforward to disentangle the thermal spectra from the non-thermal ones. While not important for the total background, any model of a specific component is to some extent dependent on this separation.

Final thoughts

In this chapter, the nature of synchrotron radiation, and the context in which it appears in astrophysics, have been explored. The synchrotron power of a single electron is sharply peaked, but the emissivity (and by extension the intensity) of a region with a certain density of electrons is more spread out. The reason for this is that the different energies in the electron distribution correspond to different critical frequencies. The impact of the power law structure of electron spectra has also been elucidated. The mechanism that creates large scale synchrotron radiation in galaxies is that of cosmic ray electrons, propagating in the galactic magnetic fields. The power law energy dependence of the particle spectra is a result of acceleration by supernova remnants. The structure of galactic magnetic fields is quite complicated, but the impact this has on the total synchrotron emission of a galaxy can be ignored for the purposes of the thesis. Finally, the radiation itself lies in a particular frequency interval called the radio waveband. At these frequencies, synchrotron radiation coexists with thermal radiation, the latter being, e.g., emission from Hydrogen clouds. Together, these two kinds of radiation make up the thermal and non-thermal components of the radio background.

It goes without saying that the details of synchrotron radiation are very important for the work to be done in the next chapter. However, the less obvious details that are important, are the electron spectra and the details of the radio background. The electron spectra are important because they directly influence the shape of the resulting synchrotron spectrum. Since one knows the desired shape of the synchrotron spectrum in advance, one needs to adapt the electron spectrum correspondingly. At the same time, it is important to maintain a realistic model for the distribution of cosmic ray electrons. The main calculation to be done in the next chapter is finding the total synchrotron background. Hence, it is important to separate out this component from the total radio background. As will be demonstrated, this separation proved to be more challenging than expected.

Chapter 3:

The extra-galactic synchrotron background from normal spiral galaxies

In the previous chapter, the theoretical background required for the calculation of synchrotron radiation from a distribution of electrons, as well as the environment in which such radiation and such distributions occur, were discussed. Additionally, some other constituents of the radio background was presented. In this chapter, this is used to analyze the case of the 'ARCADE excess', and to determine whether this excess might be consistent with extra-galactic synchrotron radiation from normal spiral galaxies. The motivation for this is the alternative dark matter interpretation that will be presented below.

3.1 The ARCADE excess

The Absolute Radiometer for Cosmology, Astrophysics, and Diffuse Emission (ARCADE) [29] is a balloon-borne experiment whose purpose is to measure the CMB at centimeter wavelengths. The second generation of this experiment (ARCADE 2), also measured the temperature of the galactic and extra-galactic emission [58]. This was done at six frequencies between 3 and 90 GHz. Temperature in this context, refers to the brightness temperature of the emission, which is defined as the temperature the source would have if it was a black body. In particular, by (2.21):

$$I_\nu = \frac{2h\nu^3}{c^2}\left[\exp\left(\frac{h\nu}{k_B T_b}\right) - 1\right]^{-1},$$

one can find the brightness temperature by inverting the expression above. Often the Rayleigh Jeans law will suffice, and a simple expression results from (2.22):

$$T_b(\nu) = \frac{I_\nu c^2}{2k_B \nu^2}. \tag{3.1}$$

The ARCADE 2 data revealed an excess flux after subtraction of the known galactic and extra-galactic emission [18]. Using also data from other surveys at lower frequencies, down to about 22 MHz, the following power law for the temperature was found:

$$T(\nu) = T_R \left(\frac{\nu}{\nu_0} \right)^{-\beta}, \tag{3.2}$$

where $T_R = 1.19 \pm 0.14K, \beta = 2.62 \pm 0.04$ and the CMB component has been left out.

Several explanations in terms of astrophysical sources have been explored, but they have been found unable to account for the excess [30, 56, 59]. Specifically, both the contribution from galactic sources and many of the usual candidates in terms of extra-galactic sources have been excluded. The extra-galactic sources considered are mostly discrete radio sources like radio galaxies, but some diffuse sources like synchrotron radiation from clusters and the intergalactic medium have also been explored. Thus, the origin of the excess remains hidden. This has prompted more exotic explanations. In particular, one possibility is an origin in dark matter.

3.1.1 A dark matter interpretation?

In several papers by Fornengo et al. [19, 20, 21], the possibility that dark matter might be the cause of the excess was explored, and found to be viable. The mechanism for this is through particle-anti-particle annihilations, or decay, of a light WIMP (10 or 25 GeV), and subsequent production of electrons and/or positrons. They discuss a case where the decay or annihilation produces mostly muons, which in turn produce the electrons. This is because the electron spectrum required to account for the excess must be hard, and production through muons accomplishes this. Furthermore, they found that the dark matter particle would have to have a large branching ratio into leptons. In any case, electrons from such a reaction could then produce synchrotron radiation if they are deflected by the magnetic field inside galaxies, as in the case of cosmic rays. The synchrotron radiation from electrons produced in this manner was found to be in reasonable agreement with the ARCADE excess, see Figure 3.1.

In particular, the case discussed above involves modeling the dark matter halo in which the reactions take place. It also entails producing an electron spectrum from a transport (diffusion) equation involving source terms derived from particle reactions. The halo has an impact in terms of the density of dark matter and the amount found in substructures, while the electron spectrum determines the shape of the synchrotron spectrum (as one would expect).

3.2 The total diffuse extra-galactic synchrotron intensity

As discussed above, dark matter could produce the required flux through synchrotron radiation from electrons produced by annihilations or decays, but what about the normal synchrotron background? It could be that the cosmic rays propagating in normal galaxies, generating modest

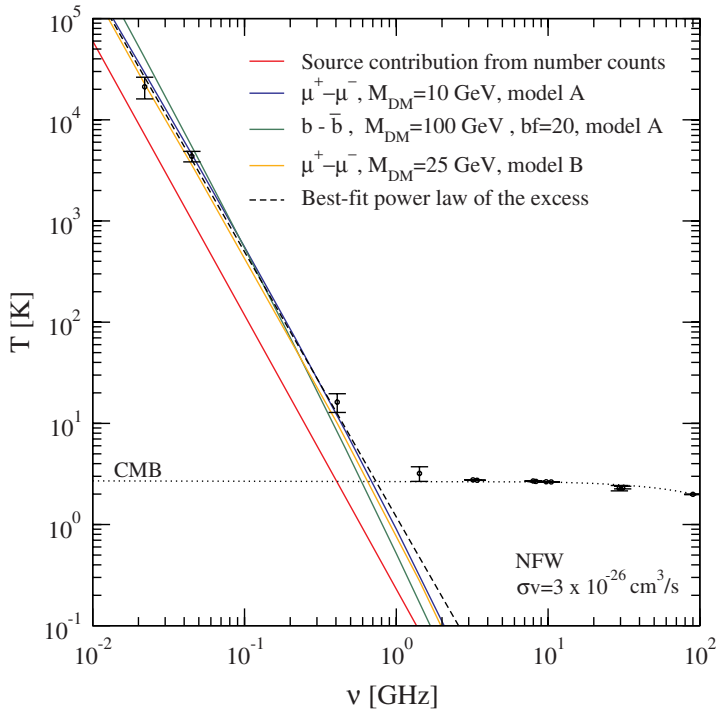

Figure 3.1: The ARCADE excess temperature plotted with a few dark matter scenarios and the astrophysical background from discrete sources, from [19].

amounts of synchrotron radiation, actually make a significant contribution when considering the entire population of such galaxies in the Universe. This case will now be studied in detail.

The total isotropic intensity per solid angle at a frequency ν, from sources with luminosity per unit frequency $\mathcal{L}_\nu$ and the comoving density of such sources in the Universe being n, is given by [20]

$$\nu I_\nu^{\rm tot} = \frac{\nu c}{4\pi}\int_0^\infty \frac{{\rm d}z}{(1+z)H(z)}\, n(z)\mathcal{L}_\nu(\nu'), \tag{3.3}$$

where $\nu' \equiv (1+z)\nu$ is the redshifted intensity and H is the Hubble parameter. In principle there will be a maximum redshift above which there is little or no contribution. The comoving number density is defined in such a way as to remain constant with redshift, if the sources are constant with redshift. Specifically, it is related to the physical number density as:

$$n(z) = \frac{n_{\rm phys}(z)}{(1+z)^3},$$

where the physical number density evolves with redshift as $n_{\rm phys} \propto (1+z)^3$ if no other redshift dependence is present. For the case of spiral galaxies, there will be a further redshift-correction related to the star-formation rate, to be discussed later. Thus, the quantities that need to be explored in detail to perform the calculation displayed in (3.3), are the luminosity and the density

of sources.

3.2.1 The synchrotron luminosity of a galaxy

In the previous chapter, an expression was derived for the intensity of synchrotron radiation from a source with a certain number density of electrons. In particular, the expression was found assuming little or no absorption. How good is this assumption for the case of a galaxy? As was discussed in section 2.3.2, observations of the Milky Way synchrotron spectrum indicate that synchrotron self-absorption becomes important below a few MHz. Since only spiral galaxies contribute to the diffuse radio background (ellipticals have little or no star-formation [51]), one need only ask whether they share this property with the Milky Way. There seem to be no indications [14] that the Milky Way is particularly special in this regard. Even so, assuming that for some galaxies self-absorption might be important up to say 10 MHz, this will not be a problem since the important frequencies for the ARCADE excess is between about 20 MHz and a few GHz. Consequently, it is safe to proceed with the assumption that, at the frequencies of interest, spiral galaxies are optically thin to synchrotron radiation.

It follows that (2.18) may be used, but this presents the question of what electron distribution should be utilized. Since the electrons are cosmic rays, the distribution should be a power law. Furthermore, the spectral index of the excess suggests an index for the power law. By (3.1) and (2.19), it is clear that the spectral index of the brightness temperature is related to that of the intensity as

$$\beta = 2 + \alpha. \tag{3.4}$$

This implies that the corresponding electron index p, should be 2.24. Additionally, as was also discussed in section 2.3.2, there should be a break in the power law at a few GeV. By putting all this together, the shape of the spectrum is determined. While the value for p below the break is set by requiring that it corresponds to the spectral index of ARCADE, the exact energy at which the break occurs and the value of p above the break, must be set. In this case, these parameters have been set by trying to get the best fit to the shape of ARCADE, while also being somewhat within the bounds set by experiments. As a result, the chosen values are 4.0 GeV for the break energy and a change in p by 1.6 (going from 2.24 to 3.84). Both the break energy and the change in p are within the error of the ones obtained by Bringmann et al. [12].

While the shape is the more immediate property to ascertain, it is eventually also important to find the correct numerical value, meaning to set the correct normalization. Though it may seem a difficult task without careful measurement of galactic synchrotron and cosmic ray spectra, one can instead use measurements of the total radio flux from a galaxy. If the synchrotron component, or rather the non-thermal component of which synchrotron radiation is the dominant sub-component, can be disentangled from the total flux, the total synchrotron luminosity can be found. Knowing what the total synchrotron luminosity should be, one can fix the normalization of the luminosity per unit frequency by integrating over all relevant frequencies. This because one has the simple relation:

$$\mathcal{L} = \int_{\nu_{\min}}^{\nu_{\max}} \mathrm{d}\nu \; \mathcal{L}_\nu. \tag{3.5}$$

Unfortunately, getting disentangled radio fluxes has proven to be a challenge. While some exist, they are incomplete selections of the available galaxies in the sky and therefore may be biased. The simplest way is of course to once again assume that all spiral galaxies are more or less like the Milky Way. This proves particularly simple because there are experimental data fixing the total synchrotron luminosity directly. However, this assumption appears to come at too high a cost in terms of accuracy and to be not all that realistic. Consequently, some work must be put into finding a distribution of galactic radio fluxes as unbiased as possible, while at the same time being able to separate the thermal and non-thermal components. Succeeding in this endeavor, one might use this distribution to make a weighted sum of galactic synchrotron luminosity normalizations to represent all spiral galaxies in the Universe.

A survey of radio fluxes that does separate between thermal and non-thermal radiation is the one by Niklas et al. [41, 42]. They collected data on a subset of the Revised Shapley-Ames catalog [55], in particular a subset of the sample observed by Condon [13]. In the Condon sample, the selection criteria is simply one of declination ($\delta \geq -45°$) and brightness ($B_T \leq +12$). Condon also added seven galaxies to the sample for completeness reasons, making the total number of galaxies 313. From the Condon sample, Niklas et al. made the further selections of $\delta \geq -25°$ and, because this was a survey at 10.55 GHz while the Condon survey was at 1.49 GHz, removing galaxies with a flux at 1.49 GHz of less than 10 mJy. This is because the steepness of the spectra make galaxies with sufficiently low flux at 1.49 GHz very hard to detect at 10.55 GHz. Additionally, two more galaxies were removed due to lack of detail. Four galaxies not in the Condon sample (though still in the Revised Shapley-Ames catalog) with brightness in slight excess of the limit set by Condon were added for unstated reasons, giving a final number of 222 galaxies. From these 222 galaxies, only a subset of the obtained fluxes were separated into thermal and non-thermal components. In particular, only those galaxies where the relative error in the fluxes were less than 15%, and those with fluxes at more than three frequencies above 400 MHz, were selected. After these reductions, 74 galaxies remained for more detailed study.

The measurements were then used to separate the radio fluxes into thermal and non-thermal components. The parameters used being the thermal fraction, f_{th}, and the non-thermal spectral index, α_{nth}. The fractional total spectrum at a frequency ν, compared to the measured value at a reference frequency ν_0, is then given by:

$$\frac{S_\nu}{S_{\nu_0}} = f_{\mathrm{th}}^{\nu_0} \left(\frac{\nu}{\nu_0}\right)^{-0.1} + (1 - f_{\mathrm{th}}^{\nu_0}) \left(\frac{\nu}{\nu_0}\right)^{-\alpha_{\mathrm{nth}}}. \tag{3.6}$$

In this case, the reference frequency is 1 GHz. This makes it quite easy to get the non-thermal spectrum by simply ignoring the first term. The luminosity per unit frequency is then found by using the redshift-independent distance to the galaxy (found in the NASA/IPAC Extragalactic Database) and multiplying the flux by the area of the corresponding sphere.

Using (3.5) to get the total luminosities for all the galaxies, one can display the distribution

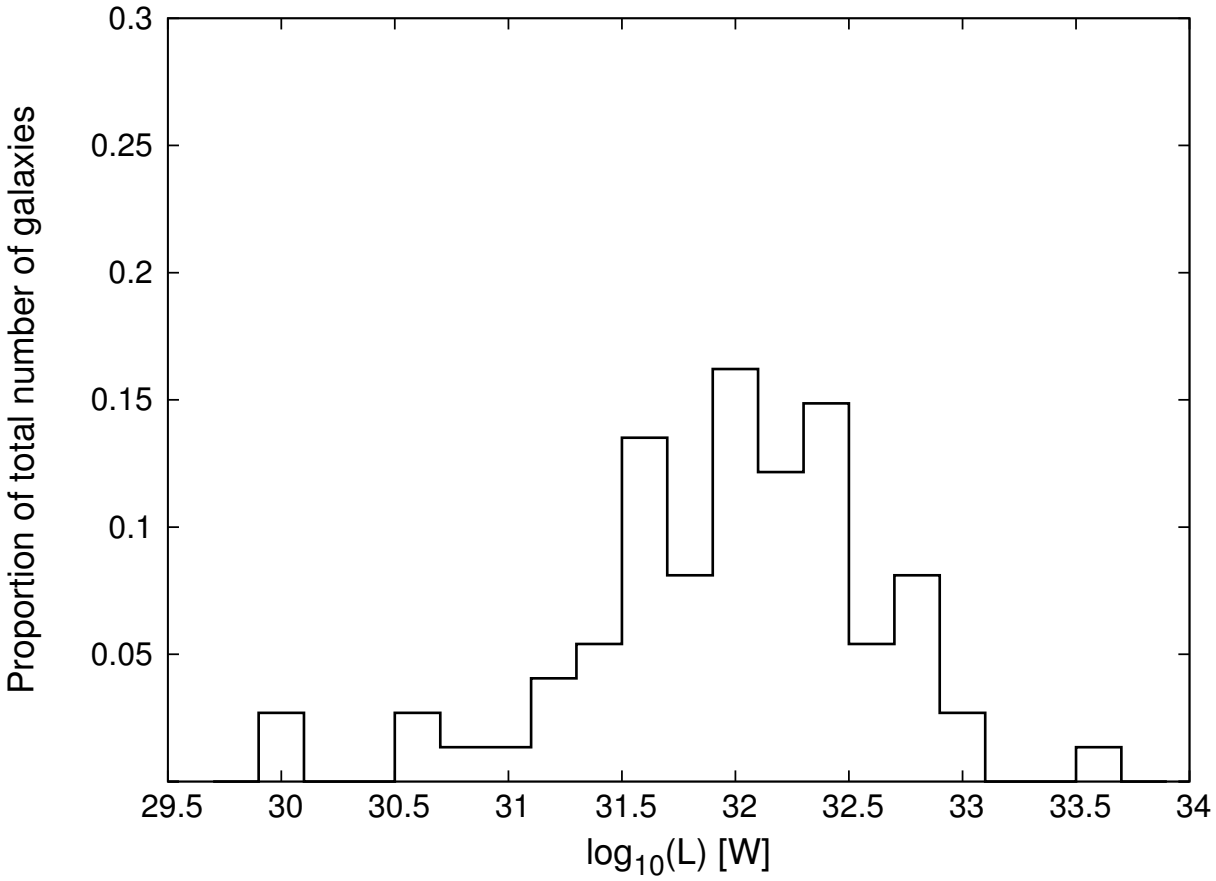

Figure 3.2: Distribution of total synchrotron luminosities for the Niklas et al. sample, using the smallest value for the bounded $f_{\mathrm{th}}^{1\mathrm{GHz}}$ cases.

of different luminosities as a histogram, see Figure 3.2. Clearly there is quite some spread, suggesting that the naive assumption of using the Milky Way synchrotron luminosity for all galaxies is not very good. Note that the Milky Way would be in the bin to the left of 31.5 in this histogram. In theory one could proceed with this distribution, using the number in each bin as a fraction of the total number as a weight for the value represented by the bin. Summing up these logarithmic contributions and taking 10 to the power of the result, gives the total normalization. Unfortunately there are some complications with this.

Firstly, the level of uncertainty in a few of the values found for the thermal fraction is quite high. The error sometimes being the same as the actual value for the thermal fraction (e.g., 0.02 ± 0.02). While this could make one question the validity of any result derived using these measurements, such a level of uncertainty does not appear in all the data. Furthermore, the number of data points should mean that any variation caused by uncertainty ought to smoothen out when all data points are included. Beyond this though, there are also some values for the thermal fraction with upper bounds only. According to the authors, this corresponds to points where the χ^2-fitting method gave the lowest χ^2-value for $f_{\mathrm{th}}^{1\mathrm{GHz}} = 0$. To address this issue, three different cases have been considered. The first case is the assumption that the thermal fraction is really small, setting it to a value that basically corresponds to zero (0.001). This was already displayed in Figure 3.2. The second case assumes the maximum value allowed by the upper bound, see Figure 3.3. Finally, the third case assumes an intermediate value which is half the value in case two, see

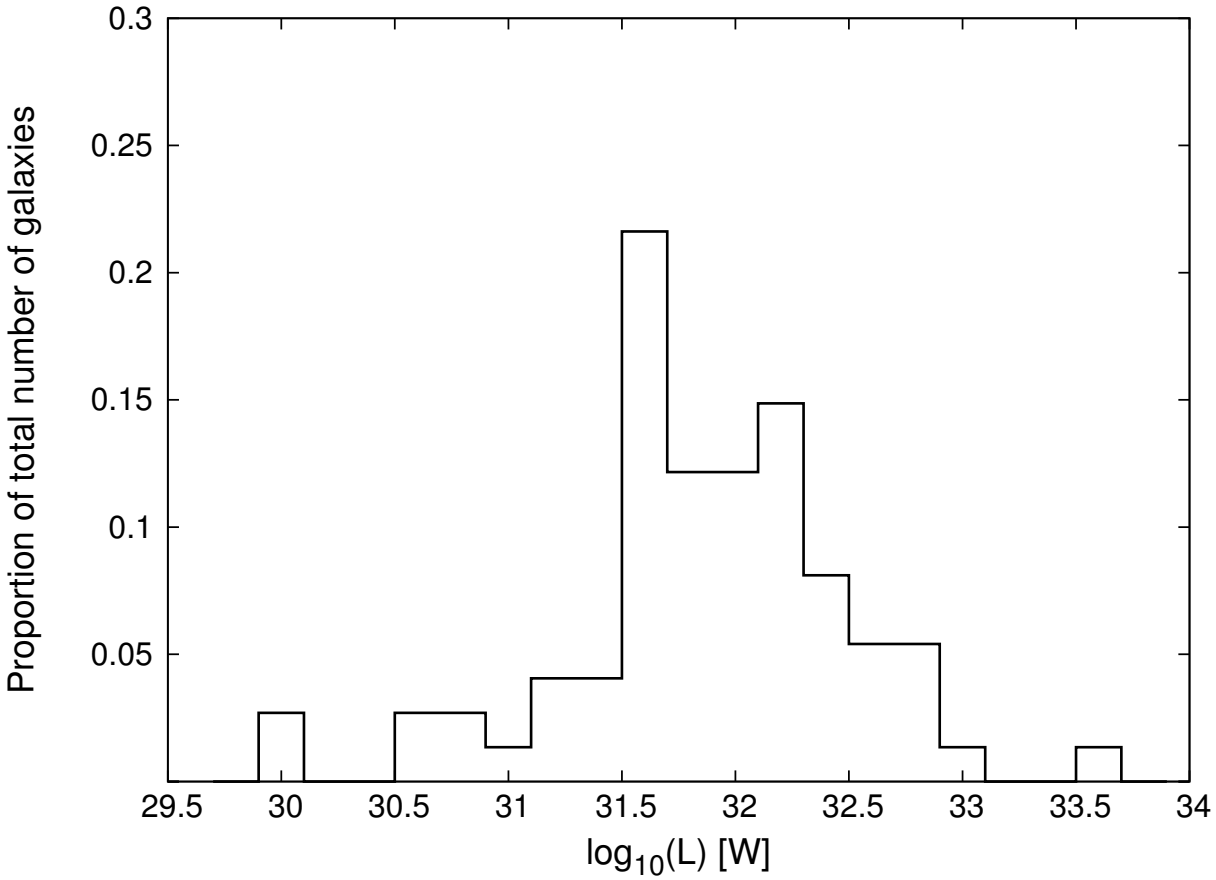

Figure 3.3: The total synchrotron luminosities for the Niklas et al. sample, using the largest value for the bounded $f_{\text{th}}^{1\text{GHz}}$ cases.

Figure 3.4. While the distributions appear somewhat different, the normalizations given by the three different assumptions are quite similar, the change being at most 30%. Hence the choice should not be very important. Finally, there are two of these thermal fractions where the upper bound is so low that the value was simply set to zero in all three cases.

As discussed above, this survey did not include galaxies with a flux less than 10 mJy at 1 GHz. The result is a potential bias towards high flux galaxies, which must be investigated. To this end, the 1.49 GHz luminosities of the entire Condon catalog can be compared with the values for the galaxies found in the sample used by Niklas et al. Specifically, using only the values from the Condon catalog and calculating the 1.49 GHz luminosity per unit frequency for all of them, histograms for the entire catalog and the sample can be shown superimposed. This is displayed in Figure 3.5. Note that the four galaxies in the Niklas et al. sample that were not in the Condon sample, are not displayed. There is nothing remarkable about these galaxies though, so their exclusion should have no impact on the interpretation of the histograms. In any case, the bias towards higher fluxes in the sample is clear. Additionally, because of the lower sample size, the distribution is narrower in general, and more sharply peaked in particular, in the case of the Niklas galaxies. While the latter might not be an issue, the high flux bias gives a normalization roughly six times larger than the Condon sample.

Another option is to use the Condon catalog fluxes and corresponding 1.49 GHz luminosities,

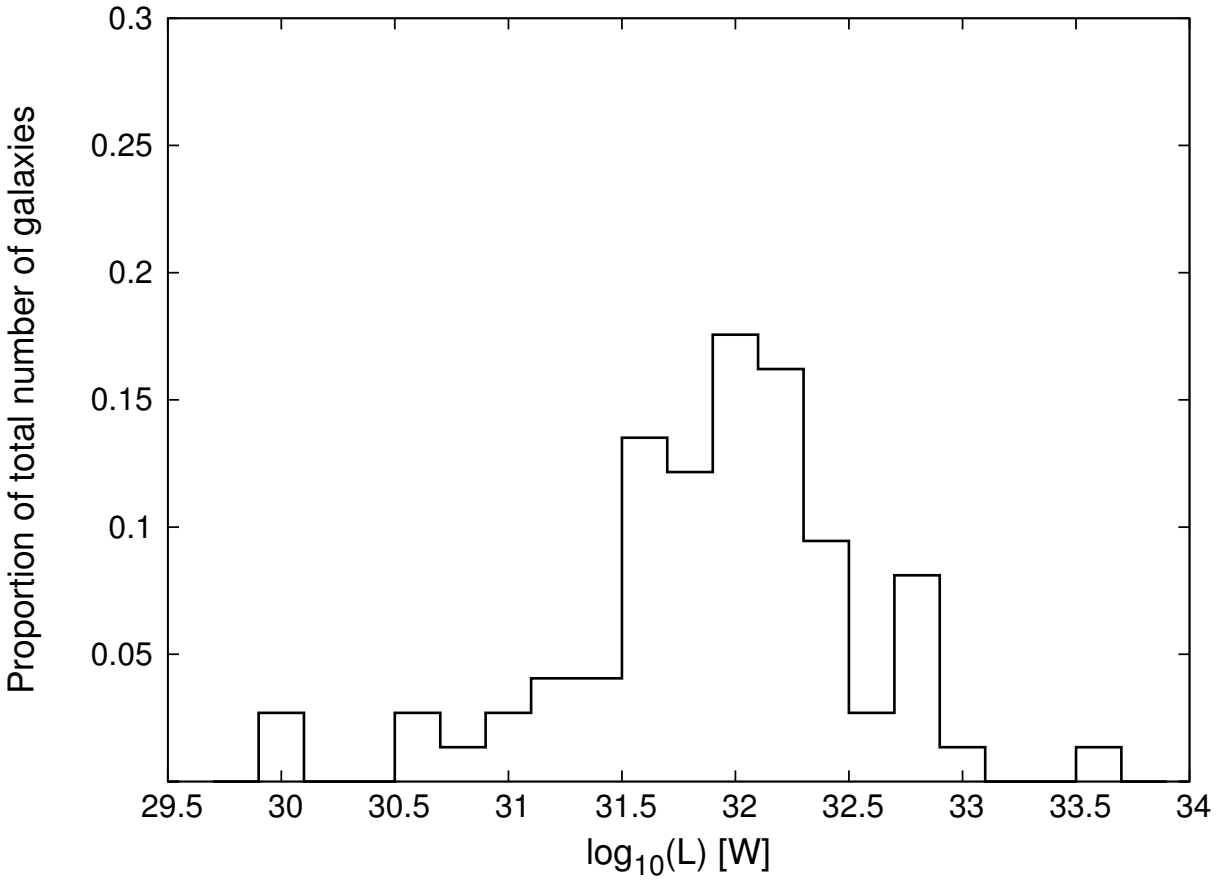

Figure 3.4: The total synchrotron luminosities for the Niklas et al. sample, using the intermediate value for the bounded $f_{\text{th}}^{1\text{GHz}}$ cases.

assuming that the average thermal fraction found in [42], 0.08, is valid for all the galaxies. This requires a slightly different scheme, using the value at 1.49 GHz to normalize, rather than the integrated luminosity. Of course, while this removes the high flux bias, it loses accuracy due to the underlying assumption. To have the average thermal fraction be a valid approximation for all galaxies, there would have to be no correlation between flux and thermal fraction. This can be investigated by calculating the correlation coefficient between the flux and thermal fraction in the Niklas et al. sample. For the sake of diligence, the three different assumptions for the bounded only thermal fractions should be considered separately. A scatter plot of the fluxes versus thermal fractions for each case is shown in Figure 3.6, Figure 3.7 and Figure 3.8. The corresponding correlation coefficients are displayed in Table 3.1.

The correlation is fairly modest in all three cases, but a bit smaller still in the former one. From the plots, the main correlation visible is the fact that the maximum value for the thermal fraction in each small flux interval gradually decreases, implying a slight anti-correlation between flux and thermal fraction. This is supported by the numerical values found for the correlation coefficients. The reason why the correlation is smaller for the first case could be that, seemingly by chance, most of the undetermined thermal fractions are at the lower half of the flux distribution. Hence, using the smallest value contributes counteractively to the observed anti-correlation. This is reinforced by the fact that the large value case has a slightly higher correlation than the intermediate case. Overall, it does not seem that any of the three assumptions substantially

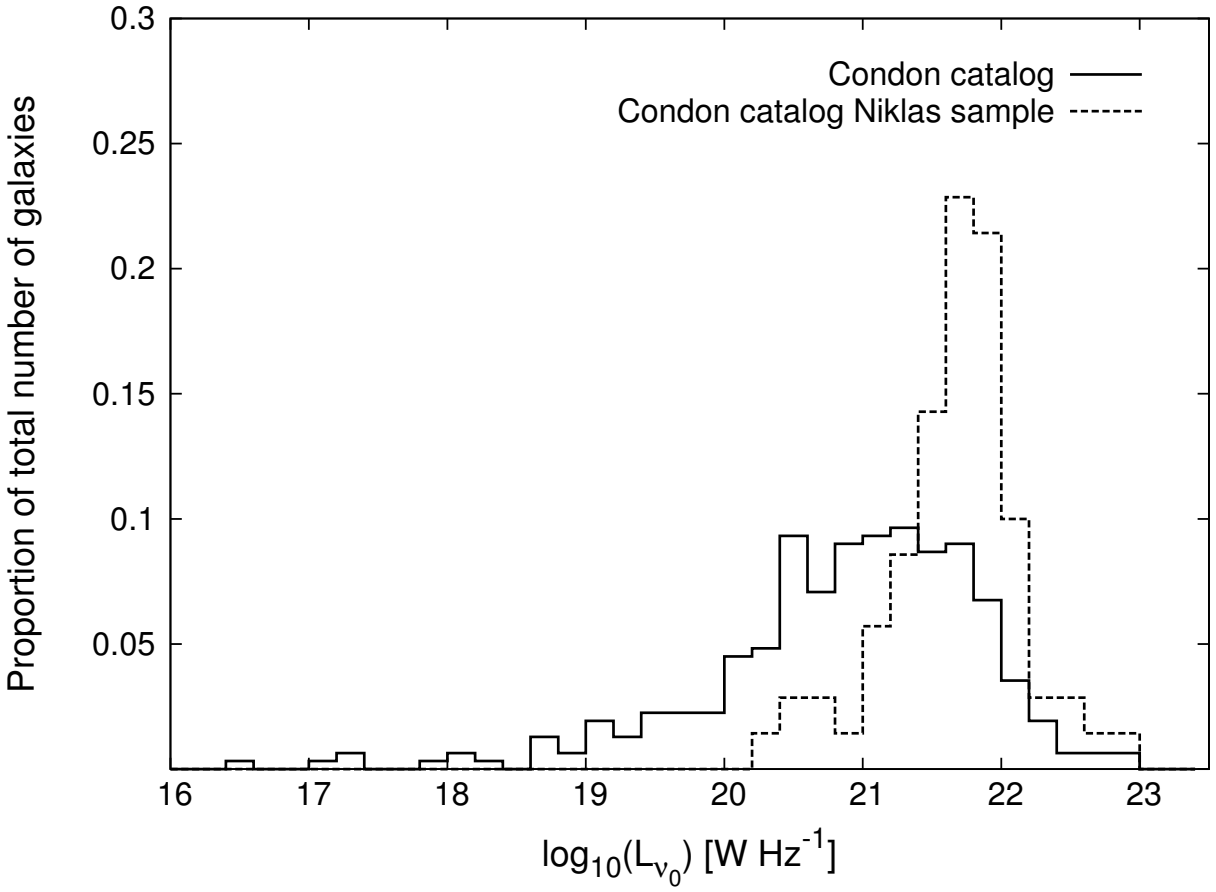

Figure 3.5: Normalized histograms for the Condon catalog [13], showing the luminosity per unit frequency at 1.49 GHz for all galaxies (solid line) and those also in the Niklas sample only (dashed line).

changes whether or not the assumption of low or no correlation is fair. In general, the variance of the thermal fraction is more or less the same for most flux values, the main deviation being at the high flux end of the distribution where the number of points is low anyway. The final interpretation is that, while there is some (anti-)correlation between the two quantities, assuming a common average value for the thermal fraction should be a fair approximation for most of the flux values. Slightly higher accuracy might be possible by adjusting the thermal fraction at the high flux tail, though the overall impact will be very small considering the intended purpose.

In conclusion, the choice seems to be between a slight high flux bias, but higher accuracy, and possible inaccuracy in the calculated non-thermal fluxes, but better statistics. Since the effect is only a change in a single number, both cases can be used and the outcome compared. While they give noticeably different values for the normalization, the values are close enough to be within the tolerance one might be expected to set, given the necessary reliance on these somewhat uncertain measurements.

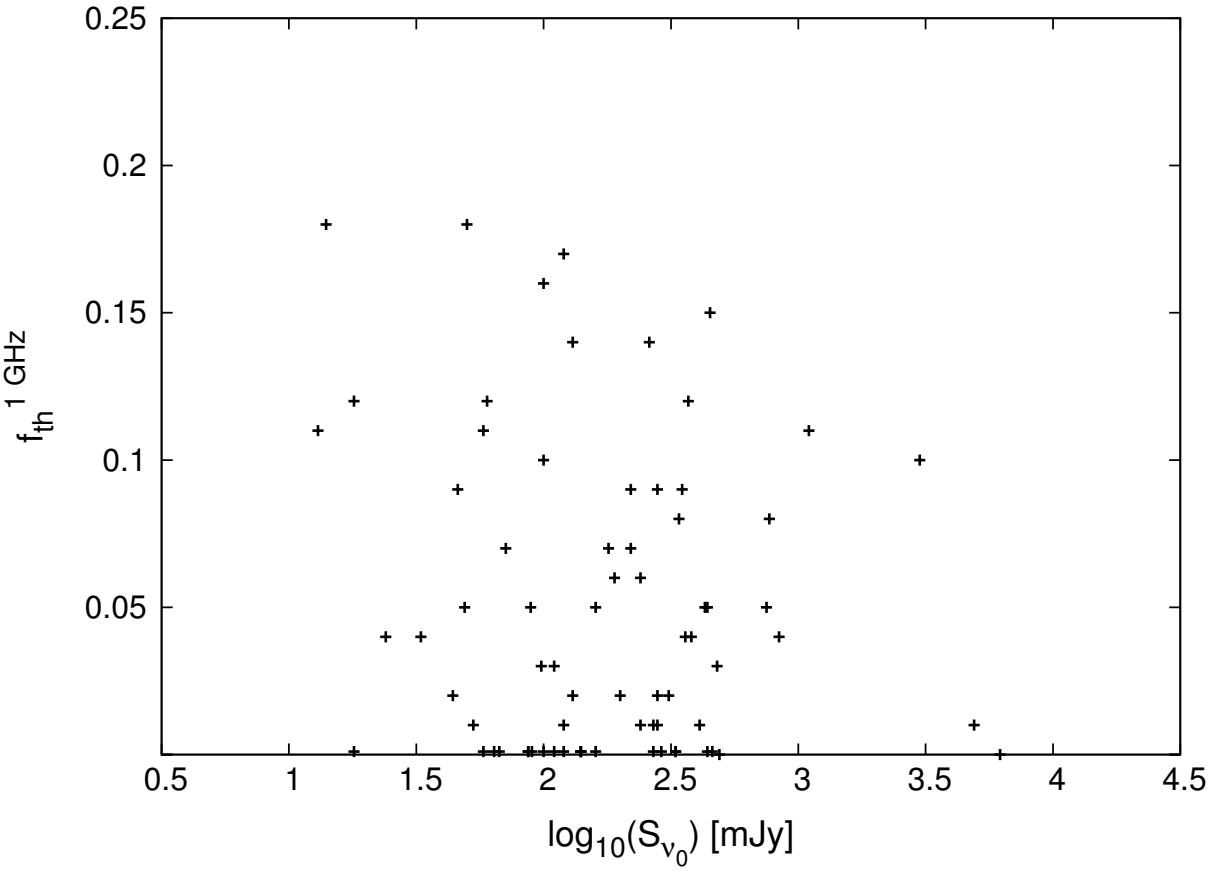

Figure 3.6: 1 GHz flux of Niklas sample plotted against thermal fraction, smallest value for the bounded thermal fractions.

3.2.2 Redshift evolution of the sources

The other important factor in (3.3) is n, which contains information about the evolution of the sources with redshift. In particular, one expects that for synchrotron sources, the dependence should be the same as for the cosmic star-formation rate in galaxies. This is because the production mechanism of the cosmic rays responsible for the synchrotron radiation, supernovae remnants, is closely tied to the star-formation rate. The higher the star-formation rate, the more stars that become supernovae are created, giving a higher cosmic ray density. The evolution of the star-formation rate is a power law in redshift up to somewhere between redshift 1 and 2, where it flattens. Beyond this, the number of potential sources remains constant. This lasts until the point where one expects the number of galaxies to start dropping off significantly, because

Table 3.1: Correlation coefficient between luminosity and thermal fraction for different values of the bounded thermal fractions.

Choice for bounded thermal fractions	**Correlation coefficient**
Smallest value	-0.157
Largest value	-0.280
Intermediate value	-0.240

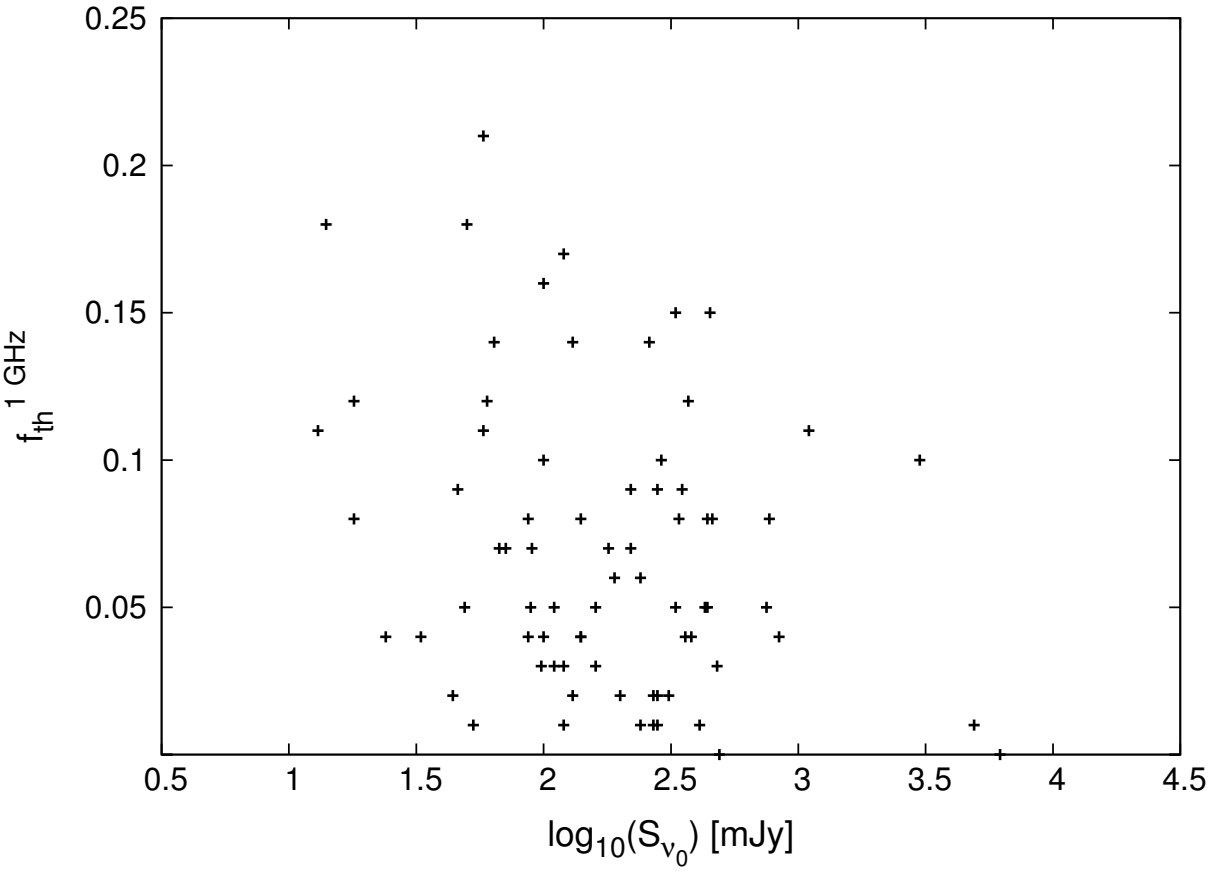

Figure 3.7: 1 GHz flux of Niklas sample plotted against thermal fraction, largest value for the bounded thermal fractions.

not enough of them had formed yet. Observations point to the cosmic star-formation rate being larger at this high redshift plateau, than it is at present.

A specific model for the cosmic star-formation rate was derived by Strigari et al. [61]. They use a broken power law of the form:

$$R_{\mathrm{SF}}(z) = \begin{cases} R_{\mathrm{SF}}(0)\,(1+z)^{\beta} & : z < z_{\mathrm{p}} \\ R_{\mathrm{SF}}(z_{\mathrm{p}})\,(1+z)^{\alpha} & : z > z_{\mathrm{p}} \end{cases} , \tag{3.7}$$

where β was taken to be 2, α taken to be 0 and z_{p} taken to be 1. These values are all conservative ones, the uncertainty being quite large for α and z_{p}. The value for β is somewhat more constrained. While some data could allow for values up to 4, this is mostly ruled out by measurements of the neutrino background, giving an expected upper bound of 3. For α, a value around 0 is expected, but it might not be exactly zero. In the case of z_{p}, values up to 2 could in principle be allowed as well. All in all, this suggests rather than firmly sets, values for these parameters. As a consequence, a few different scenarios can be explored. The difference between the lower and upper boundary of allowed values, in terms of their effect on the overall magnitude of the intensity, is expected to be noticeable, but modest. Still, this is another case where variation caused by uncertainty in the model, from lack of complete experimental data, can influence the overall result. As such, it is important to explore the full range of possibilities.

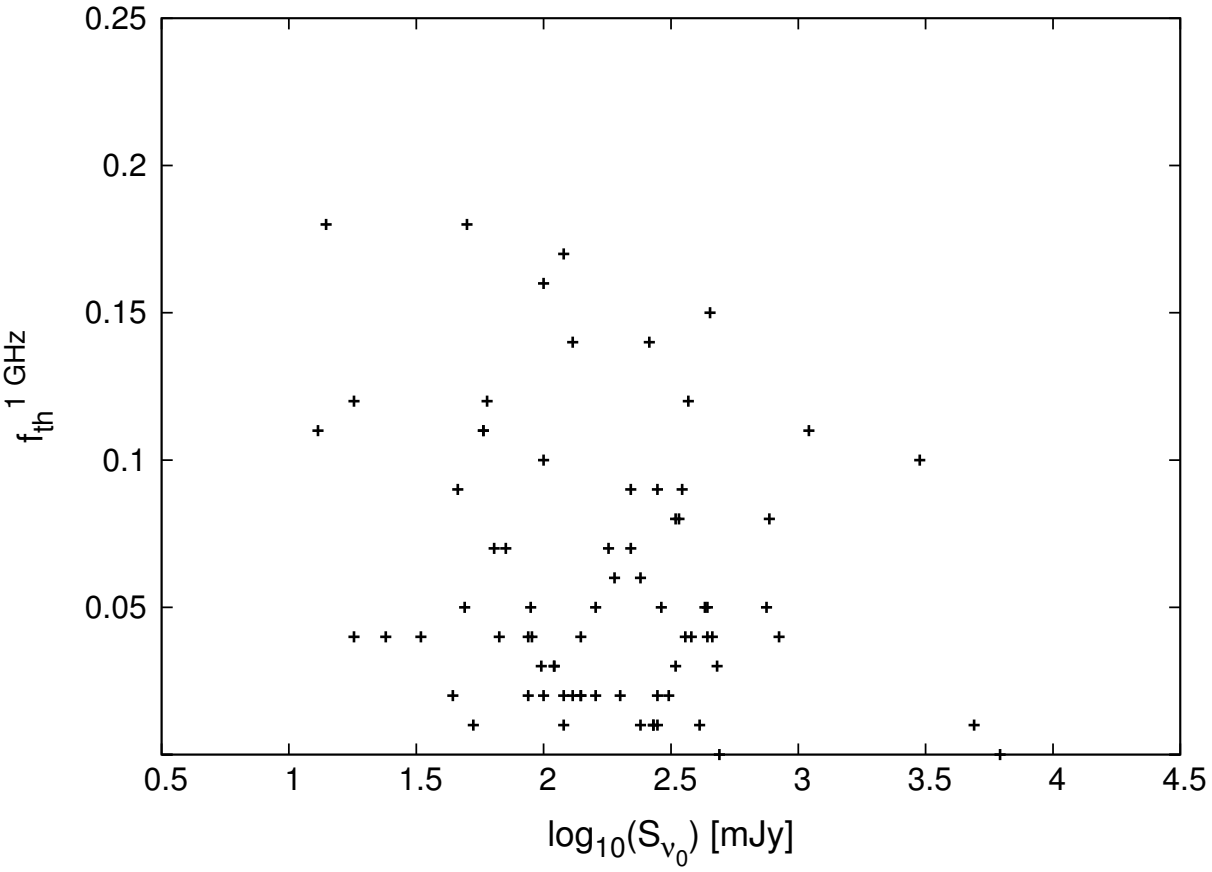

Figure 3.8: 1 GHz flux of Niklas sample plotted against thermal fraction, intermediate value for the bounded thermal fractions.

3.2.3 The final extra-galactic synchrotron intensity from spiral galaxies

The preceding discussions give a sizable parameter space to explore. The main choices for the normalization seems to be either using the complete Condon catalog, with the average thermal fraction found by Niklas et al., or that which can be derived from the model and data found by Niklas et al. only. The latter also includes the three different choices for the bounded only thermal fractions. This is already quite a few different cases to explore. Furthermore, there are also the different possible parameter values in the model for the redshift evolution of the luminosity. The main effect being that low (conservative) values for the power law and the cutoff yield lower redshift-corrected intensity, while higher (perhaps optimistic) parameter values give correspondingly higher intensity. Combined, these two sets of parameters give a non-trivial range of possible intensities. Finally, one might also investigate the effect of different values for the magnetic field and the electron spectral index. While the latter is not too relevant because of the need for a certain shape of the spectrum, it could be interesting to see the sensitivity to changes. Varying the magnetic field will modify the critical frequency and hence shift the spectrum either left or right. Neither of these change the overall normalization. All in all, there are a lot of things to consider.

Proceeding first from (3.3), the terms can be broken down as follows. The redshift evolution of the luminosities, $n(z)$, follows the cosmic star-formation rate as indicated in the previous

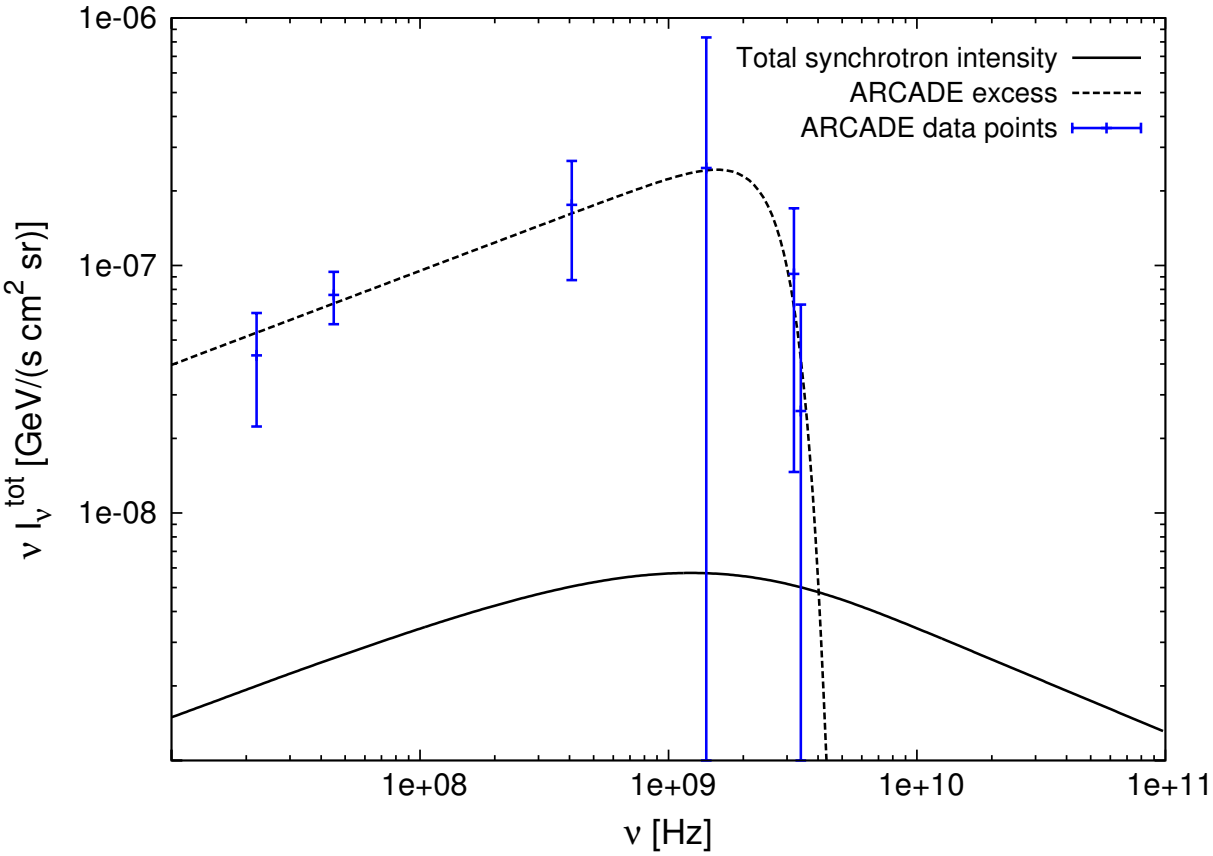

Figure 3.9: The total synchrotron intensity (solid line) compared with the excess (dashed line), using the most conservative parameters. Also shown are points (blue) computed from the data points of ARCADE and the lower frequency surveys.

section by (3.7). In particular, the redshift dependence is the same, but the normalization is not. The normalization is the present time comoving number density of spiral galaxies. This value depends on, e.g., what lower cutoff is used for the luminosity function (and of course the particular luminosity function utilized). Unfortunately, such an analysis has not been done in this case. The value is set to be $0.1/\mathrm{Mpc}^3$, which should be roughly of the right magnitude. Any corrections to this number would be a simple overall adjustment to the total normalization. There is also some challenge in separating the spiral galaxy component of the total number of galaxies. The value used here has been derived from the data found by the Galaxy Zoo collaboration [35]. Since this is a project where amateur scientists have contributed by voting for the morphology of each galaxy, there is again a certain amount of uncertainty present. Specifically, by setting the percentage threshold for when a galaxy qualifies as determined rather than unknown, the number of unknowns can be as low as a few percent or higher than 50 percent. There is also some correction for bias, where the authors have taken into account the likelihood that far-away spirals may appear as ellipticals, because the spiral structure is not clearly visible. In the end, the percentage of spiral galaxies in the Universe (extrapolated from the Galaxy Zoo data) is between 20 and 30 percent. This is another possible parameter space variation, though the difference is fairly small.

Next is the luminosity, which is the total synchrotron emission of a galaxy. This is derived from the expression for the synchrotron intensity of a single source (galaxy), found in Chapter two

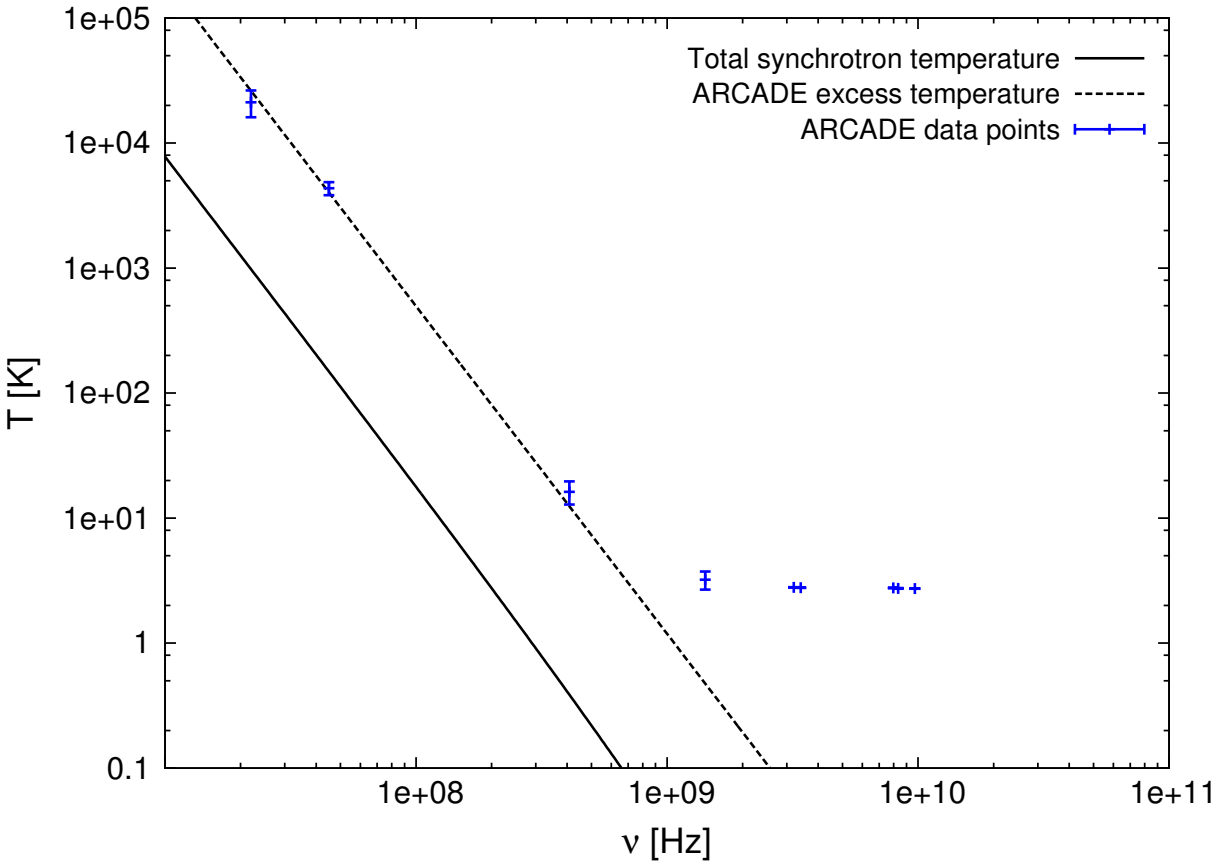

Figure 3.10: Brightness temperatures for the low parameter values of the total synchrotron intensity (solid line) and the ARCADE excess (dashed line). Also shown are the data points of ARCADE and the lower frequency surveys (blue).

(equation (2.18)). Multiplication by $4\pi R^2$, where R is the radius of the emitting region, and redshifting all frequencies $\nu \to (1+z)\,\nu$, gives the final expression for the synchrotron luminosity per unit frequency of a single galaxy. Lastly, the following expression for the Hubble parameter, valid for the assumed ΛCDM cosmology, and the values for the cosmological parameters listed in Table 1.1, is used:

$$H(z) = H_0 \left[\Omega_\Lambda + \Omega_\mathrm{m}(1+z)^3\right]^{1/2}.$$

Hence, the utilized expression for the total synchrotron intensity is:

$$\nu I_\nu^\mathrm{tot} = \begin{cases} \dfrac{\nu n_0 c}{H_0 4\pi} N \displaystyle\int_0^8 \frac{\mathrm{d}z\,(1+z)^\beta \mathcal{L}_\nu(\nu')}{(1+z)\sqrt{\Omega_\Lambda + \Omega_\mathrm{m}(1+z)^3}} & : z < z_\mathrm{p} \\ \dfrac{\nu n_0 c}{H_0 4\pi} N \displaystyle\int_0^8 \frac{\mathrm{d}z\,(1+z)^\alpha \mathcal{L}_\nu(\nu')}{(1+z)\sqrt{\Omega_\Lambda + \Omega_\mathrm{m}(1+z)^3}} & : z > z_\mathrm{p} \end{cases}, \tag{3.8}$$

where n_0 is the present time number density of spiral galaxies, N is the overall normalization of the luminosity, β, α and z_p is as given in the previous subsection, and the upper integration

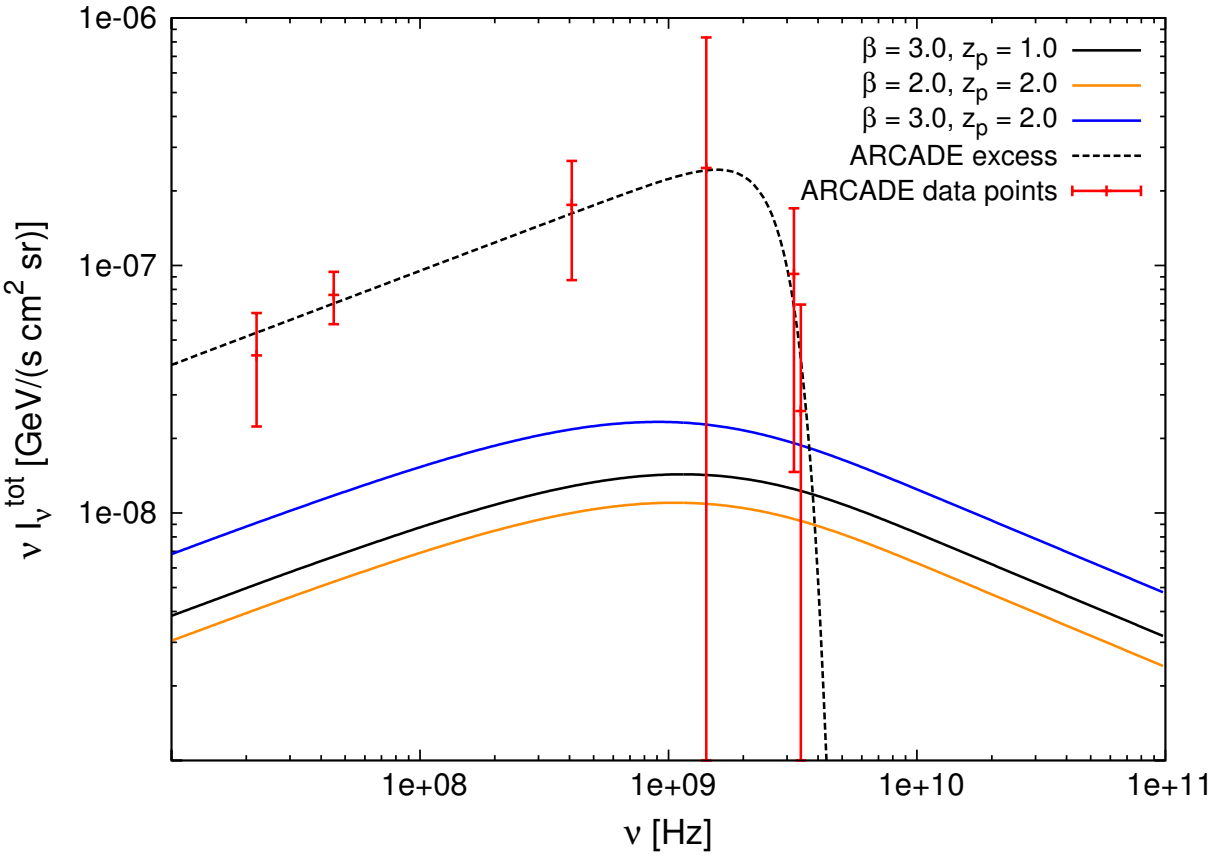

Figure 3.11: Total synchrotron intensity normalized as in figure 3.9, but with 30% spiral galaxies and variation of other parameters. Also shown are the computed data points (red).

limit has, for simplicity, been chosen to be 8; beyond which the contribution to the integral is negligible. This expression (including the luminosity found as explained above) is then evaluated numerically.

Beginning with the most conservative assumptions for all parameters, namely having the normalization of the luminosity set by the entire Condon catalog and an assumed average thermal fraction of 0.08, choosing the lowest values for the power law and cutoff of the redshift distribution, and assuming 20% spiral galaxies in the Universe, yields the result shown in Figure 3.9. The displayed ARCADE intensity is found by inserting the expression for the derived brightness temperature (see (3.2)) into the Planck law (2.21). The values chosen at this point for the magnetic field and electron spectral index are 10.0 μG (roughly the average value for spiral galaxies [5, 4]) and 2.24 (as dictated by the ARCADE spectral index) respectively. In all the following plots, the data points found by ARCADE and the mentioned lower frequency surveys [18] are displayed. In the intensity plots, the data points (being temperature) have been used to compute the corresponding intensity points. For the temperature plots, the data points are shown as reported in the mentioned article. Note that only the first three points are really part of the fit of the excess. The rest are well fitted by the CMB, see Figure 3.1 where the same points are shown. The departure from the ARCADE fit is generally more evident in the temperature plots. This also explains the apparent discrepancy beyond roughly 1 GHz in the intensity plots, the ARCADE fit represented by the Planck curve is not applicable beyond this frequency area. Despite this, all the points (and the entire Planck fit) are shown for clarity. Note also that some

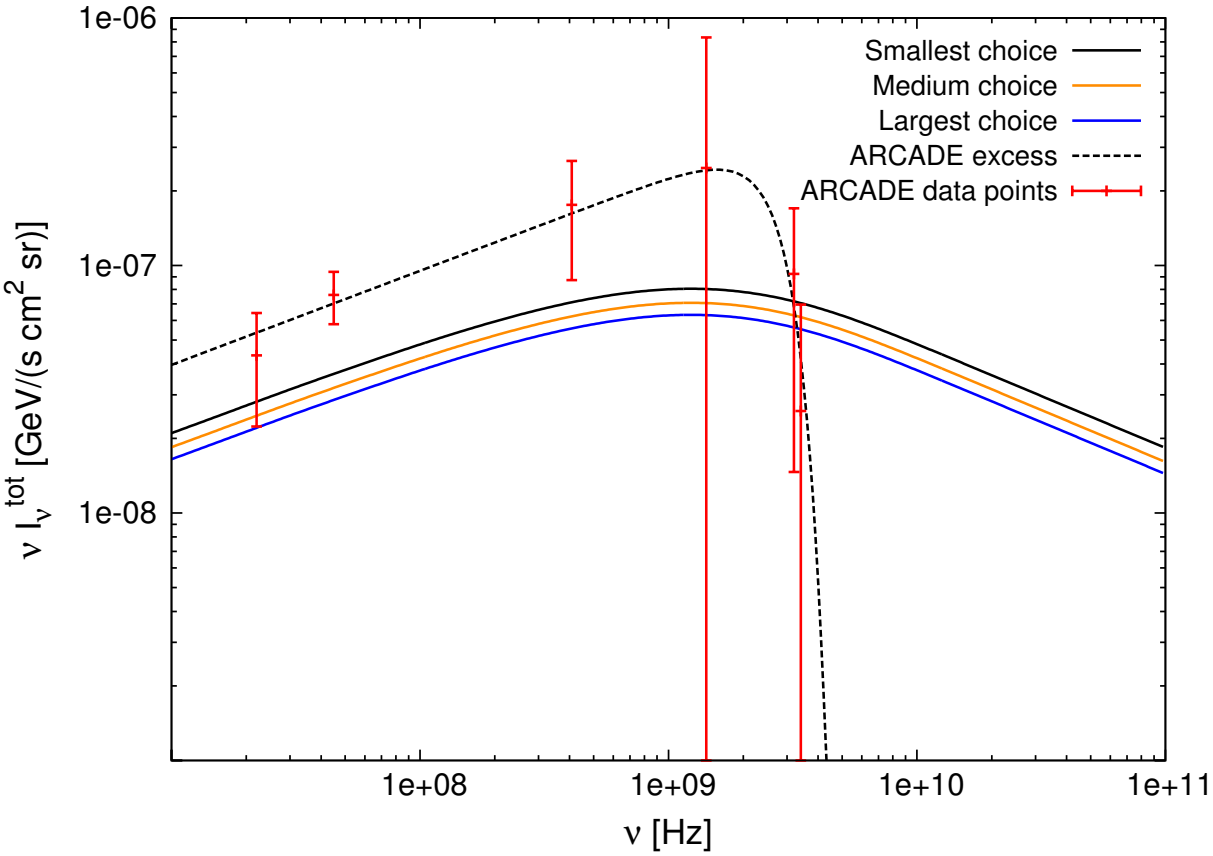

Figure 3.12: Synchrotron intensity normalized by the Niklas catalog derived luminosities, using the lowest values for the parameters. Three cases are displayed, corresponding to different values for the bounded only thermal fractions. Also shown are the computed data points (red).

of the error bars in the intensity plots extend beyond the lower bound of the plots. This is a natural consequence of the logarithmic scale and the fact that the error is of the same magnitude as the actual value.

As is evident, these parameter values gives an intensity more than an order of magnitude below ARCADE. The shape looks fairly similar (considering that the Planck law shape is an approximation for the excess) though. Clearly, the lower boundary of parameter space for the intensity cannot account for the ARCADE excess. If a plot of the corresponding brightness temperatures is made, see Figure 3.10, the similarity of the shapes becomes even more clear.

Keeping the same normalization of the luminosity and values for magnetic field and electron spectral index, but considering higher values for z_p and β, yields the intensities shown in Figure 3.11. The parameter α is kept at zero in all the plots in this chapter. Since it is known to be close to zero, this simplifies the model, but also should not lose much accuracy. The contribution from increasing the percentage of spiral galaxies only, is small. Hence, it is not shown individually. Changing the redshift evolution parameters clearly does have an effect, though. In particular, the most optimistic combination gives a very noticeable increase. However, there is still some distance up to the level of ARCADE; slightly less than one order of magnitude to be precise. From this it seems that if the average luminosity of spiral galaxies is close to that indicated by the Condon catalog fluxes, synchrotron radiation from this type of source cannot account for the

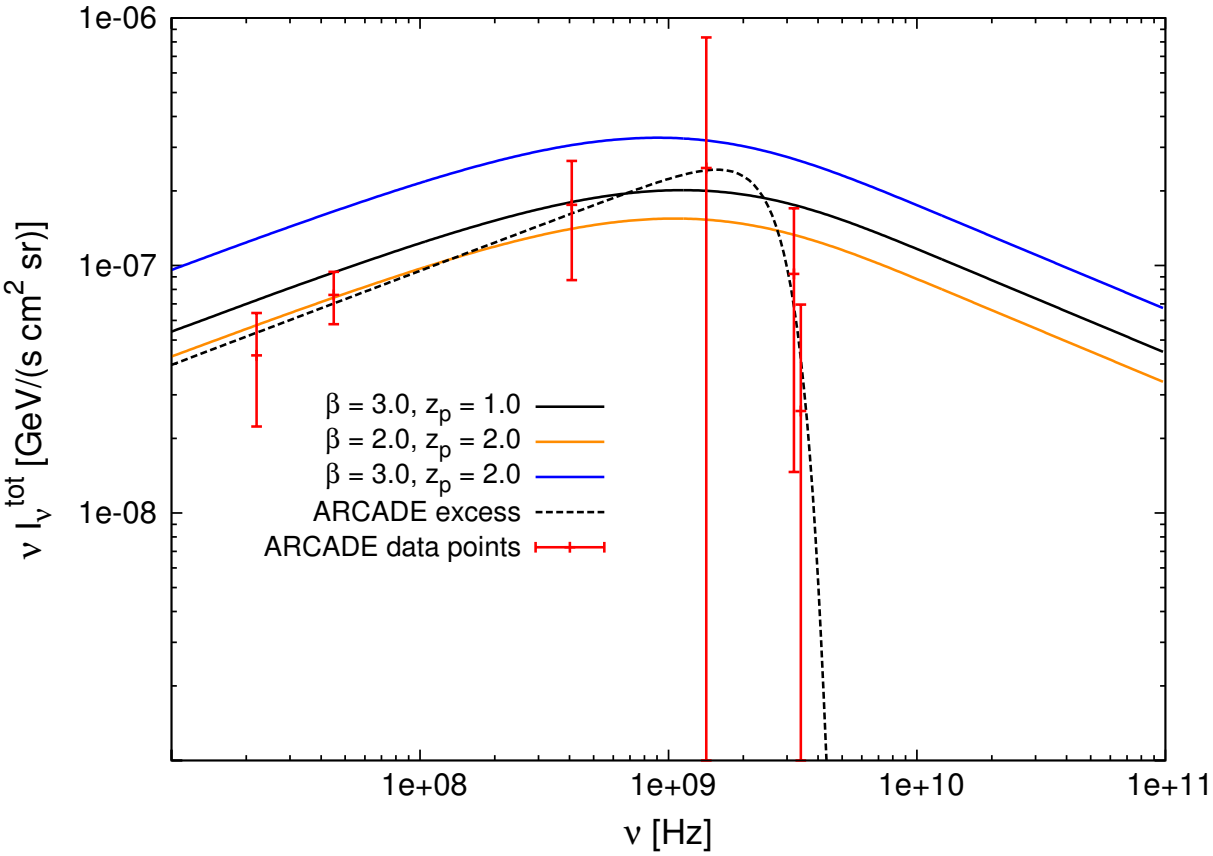

Figure 3.13: Synchrotron intensity normalized by Niklas catalog derived luminosities, using higher parameter values and 30% spiral galaxies. Only the case with the smallest value for the bounded thermal fractions is shown. Also shown are the computed data points (red).

ARCADE excess even when considering the contribution from all directions and redshifts.

Yet, this does only take into consideration the lower half of our parameter space. Having already noted the increased average luminosities indicated by the Niklas catalog, changing the overall normalization to reflect this could increase the intensity sufficiently to explain the excess. Starting again with the lower values for the parameters relating to the density and redshift evolution of the sources, the new normalization can be implemented. However, as discussed at length previously, there are three cases to consider, which are expected to give different, though similar, values for the normalization of the luminosity. Note also that the normalization scheme is slightly different for this case. Whereas previously the normalization was fixed by demanding that the calculated luminosity going into the expression for the intensity had the correct value at 1.49 GHz, here the normalization is fixed by integration over all frequencies. While the Condon catalog provided only fluxes at a certain frequency, the Niklas catalog gave also a way to get the flux (and hence the luminosity per unit frequency) at any other frequency through (3.6). The resulting spectrum could then be integrated, giving a value for the total luminosity from the relevant frequency range. Correspondingly, the calculated synchrotron luminosity was fixed so that the integral over frequency matched the average value found from the Niklas catalog galaxies. With this in mind, all three cases are displayed in Figure 3.12.

These intensities are marked improvements, though still a bit on the low side compared with

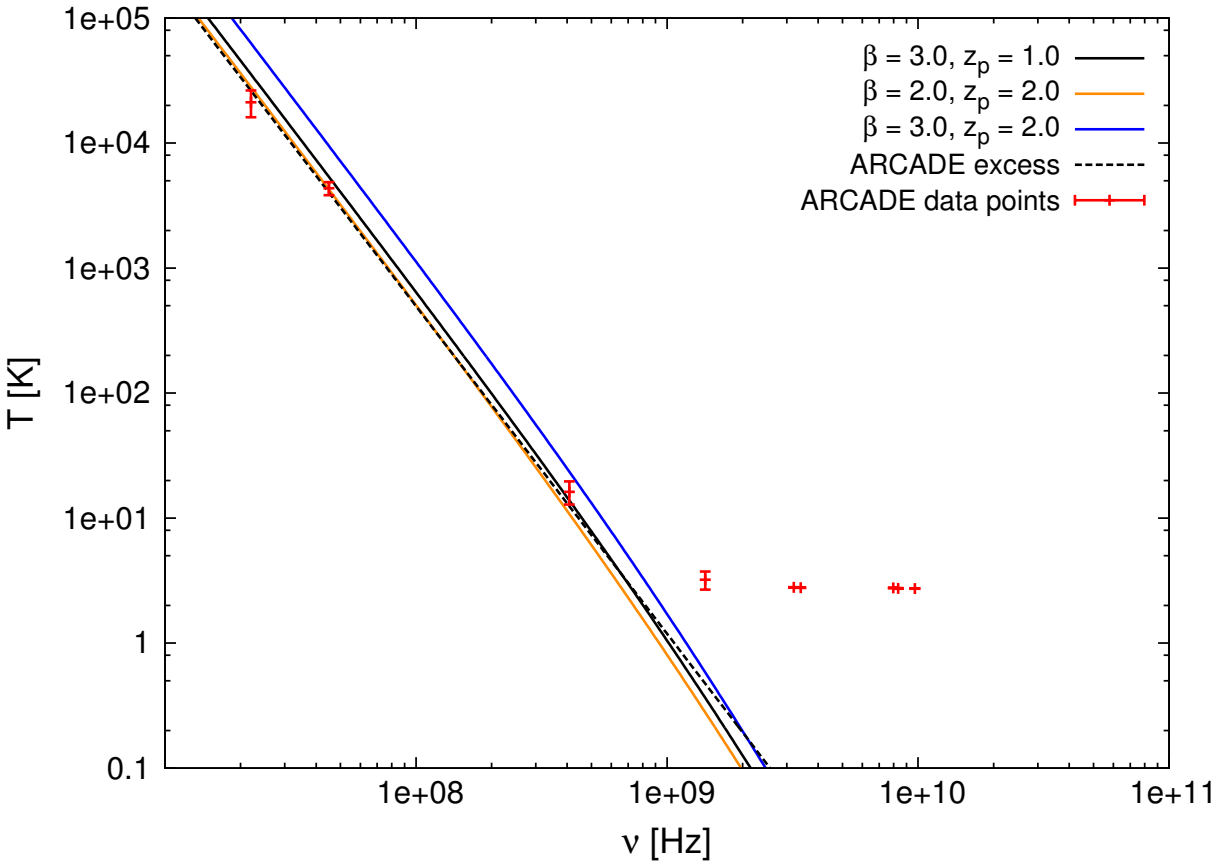

Figure 3.14: Synchrotron brightness temperatures for the intensities shown in figure 3.13 and the data points (red).

ARCADE. It is interesting to note that in the end, the differences between the three cases are rather small. Clearly not much loss in accuracy is involved by choosing one over the other. Thus, for simplicity, it is from here on assumed that the lowest thermal fraction case can be used in further calculations. Proceeding to higher parameter values, corresponding new values for the intensity are shown in Figure 3.13.

This finally gives values that are, respectively, at the same level as ARCADE, just below and just above ARCADE, the lower two both dipping below at the peak. All three cases could, within the inherent uncertainty present in some of the values used, account for the excess. Clearly, this is not very conclusive either way because of the mentioned uncertainty, which could go the other way as well. For reference, a temperature plot based on the same intensities is given in Figure 3.13, showing perhaps more clearly the fit. The electron spectral index and the magnetic field strength have remained unchanged so far. As discussed previously, they do not affect the overall normalization. Rather, they affect the shape of the intensity and have therefore been set to best fit the shape of ARCADE. For illustrative purposes, some plots with various values for these parameters are shown and discussed in Appendix A. The values chosen clearly give the best fit to the excess. The electron spectral index and the magnetic field strength are consequently set by hand to these values, and can be regarded as part of the model used in the thesis.

What can be taken away from this? Considering the fact that the Niklas sample has a high flux bias when compared to the Condon catalog, it might seem like an overstep to use the normal-

izations derived from the former, to claim that the ARCADE excess can be accommodated by synchrotron radiation from spiral galaxies. However, the knowledge of non-thermal radio fluxes from spiral galaxies is currently not complete enough to claim that doing so is to overestimate the contribution of such sources. While the statistics, as represented by the Condon catalog, is on the side of weaker fluxes, higher ones cannot presently be ruled out. So it seems possible, that synchrotron radiation from normal spiral galaxies could account for the ARCADE excess, particularly given some favorable assumptions about the redshift evolution of the sources. Again, the need for optimistic values for these parameters is certainly cause for some concern, but since they are within current bounds, the results are at worst inconclusive. Only further constraints can decide whether these parameter values are possible, or at least the likelihood of these values. This is also true for the average size of the synchrotron fluxes. Nevertheless, it is important to note that the model we have used in this thesis is very simple. The fact that such a simple model can produce results that fit the data so well at all, should not be taken for granted. So while it may not be favorable based on the current data, the possibility that the excess can be explained in the way presented in this thesis, cannot be excluded.

3.3 The angular 2-point correlation function of star-forming galaxies

One way to investigate the consequences of the adopted model for the redshift-evolution of the sources ($n(z)$ of (3.3) and subsection 3.2.2), is the corresponding angular correlation function. This is a measure of the probability of finding another galaxy (source) at a certain angle from any given galaxy in the sky. It is given by [20]:

$$w(\theta) = \int_0^\infty \mathrm{d}k\, k \int_0^\infty \mathrm{d}z\, P(k) \frac{J_0(kr\theta)}{2\pi} \left(\frac{1}{n}\frac{\mathrm{d}n}{\mathrm{d}z}\right)^2 \frac{\mathrm{d}z}{\mathrm{d}r}, \tag{3.9}$$

where k is the comoving wavenumber, P is the 3D power spectrum, J_0 is the Bessel function of the first kind of order 0 and $\mathrm{d}z/\mathrm{d}r = H(z)/c$ for a flat Universe. P describes the amount of structure found in the Universe on the scale k. To define it, the definition of the density contrast is also needed. The density contrast is the relative change in the density field:

$$\delta(\mathbf{x}) \equiv \frac{\delta\rho(\mathbf{x})}{\overline{\rho}}$$

If δ_k is the Fourier transform of the density contrast, then the 3D power spectrum is defined as:

$$P(k) = |\delta_k|^2$$

It is assumed that P is independent of redshift, which could introduce some error at large scales. All in all, the biggest challenge here is the 3D power spectrum which must be found from experimental data. In this case, the one derived by [65] was used. Additionally, because they

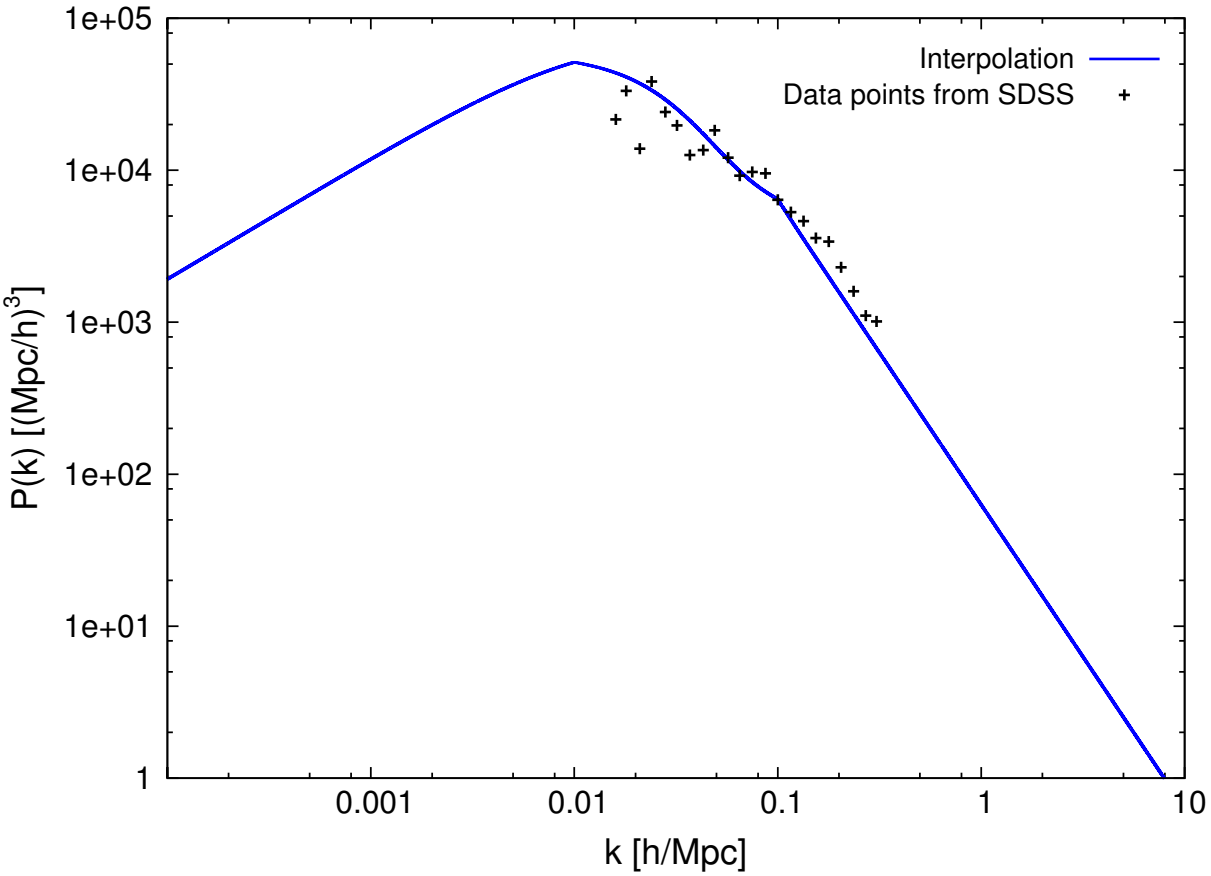

Figure 3.15: Interpolation of the 3D power spectrum shown on page 731 of [65], with the data points found by same.

only found values for a given interval of k, the overall spectrum found by comparing with other surveys (as displayed on page 731 of [65]) was used to extrapolate for both smaller and larger k-values. A plot of the interpolation of the total power spectrum as well as the points found by [65], is shown in Figure 3.15.

Furthermore, the redshift-dependence of the sources, is as previously the one taken from the cosmic star-formation rate. Reminding ourselves of the power law structure:

$$n(z) \propto (1+z)^r,$$

the contribution of the term in the parenthesis will be:

$$\left(\frac{1}{n}\frac{\mathrm{d}n}{\mathrm{d}z}\right)^2 = (r\,(1+z)^{-1})^2.$$

As a consequence, the contribution is zero above the cutoff where $r = 0$. Additionally, there were no data for the power spectrum beyond $k = 10\,h/\mathrm{Mpc}$, though clearly it goes to zero based on the trend and from physical arguments, and the contribution is very small beyond this point. The contribution should also disappear for small values, because this corresponds to very large

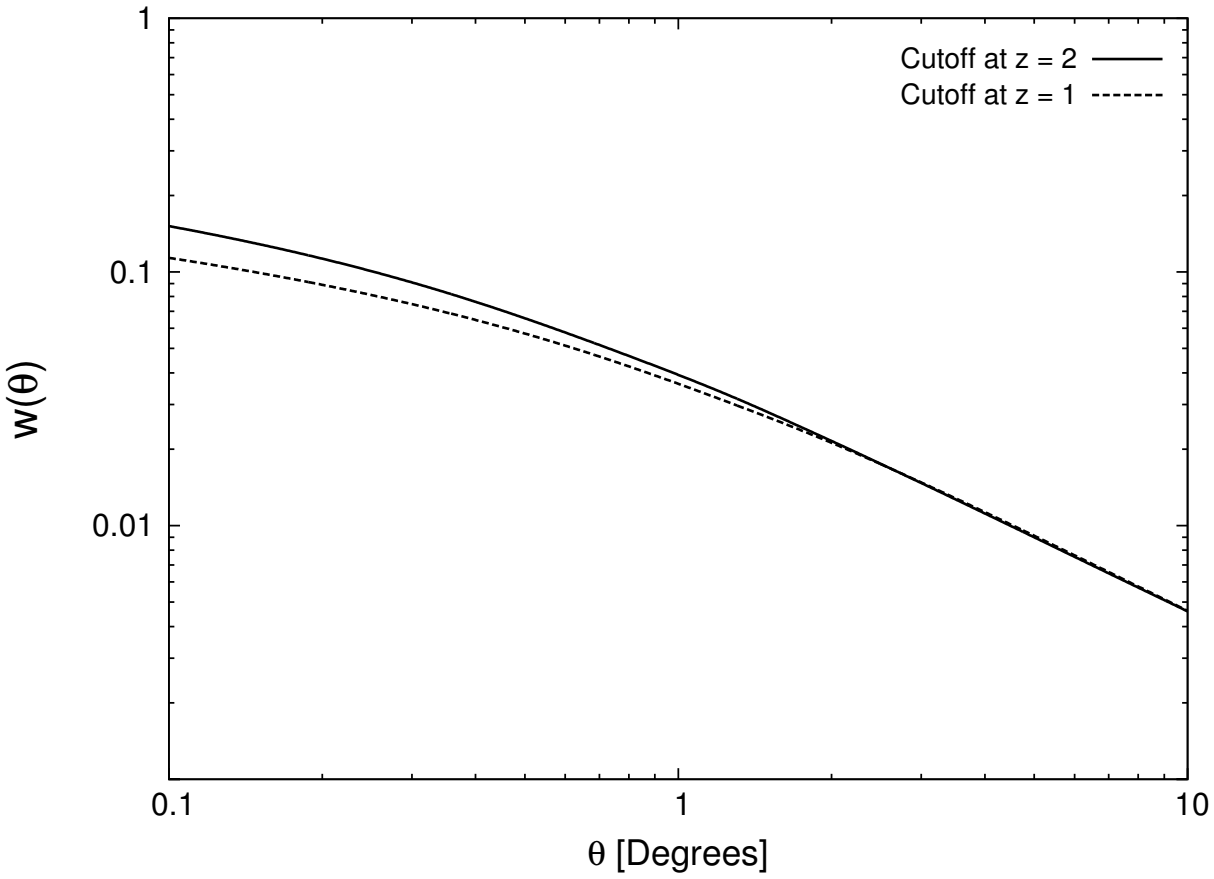

Figure 3.16: Angular 2-point correlation functions for star-forming galaxies. Redshift evolution constant above z = 2 (solid line) and z = 1 (dashed line).

scales where there should not be any structure. Hence the integration over k is taken to be over the values shown in Figure 3.15.

The remaining issue is then which parameter values to use for the cosmic star-formation rate. As was shown above, the exponent of the redshift dependence only changes the normalization. As a consequence, it is enough to plot for one fixed value of this parameter, in this case chosen to be 2.5. The cutoff value for the red shift, however, does impact the result. Thus two different values for this is used, namely $z = 1$ and $z = 2$. The resulting angular 2-point correlation functions are displayed in Figure 3.16. The difference between the two cases is relatively minor, being only present at low angles. The interpretation is that, if the redshift cutoff happens later, there are more galaxies contributing. This makes a difference at low angles where the correlation is expected to be (and indeed is) the highest for (star-forming) spiral galaxies. As one moves to larger scales the correlation becomes low enough that it makes little to no difference where the cutoff is. In general, the shape indicates a decreasing correlation with increasing angles, and a change in slope beyond roughly 1 degree. This is as one would expect for galaxies, which are more clustered together, as opposed to say dark matter (see for instance [20]) where there is a large halo around galaxies, and clusters of galaxies, which contributes also at larger angles. However, the slope is a bit too flat at large angles, compared with what one would expect. This is likely to result from the failure of the flat sky approximation at larger angles. All in all, the conclusion is that the redshift evolution of the sources being used, does give an angular

correlation corresponding to sources that are more clustered together than dark matter. While this does not give any indication of whether or not synchrotron radiation from spiral galaxies could be responsible for the ARCADE excess, it does say something. Namely where and how to look for such sources in any future experiments, should one investigate the model utilized in this thesis further. It also says that the redshift evolution utilized in the calculation in this thesis, is consistent (the inaccuracy at higher angles being due to unrelated elements) with the type of sources being studied.

Chapter 4:

Concluding remarks and outlook

In this thesis, the total synchrotron intensity from diffuse sources, in particular normal spiral galaxies, has been calculated under certain assumptions. The motivation for the work has been to investigate the possibility that this type of radio frequency radiation can account for the excess sky temperature observed by the ARCADE 2 experiment. Whereas other more conventional astrophysical sources have been excluded, one interesting suggestion put forth is an origin in dark matter. Since the mechanism through which dark matter was thought to contribute, was synchrotron radiation from electrons produced by dark matter annihilations or decays, it seems natural to ask whether the electrons already known to be present in galaxies might suffice.

Using knowledge about cosmic rays electrons in the Milky Way, a specific model for electrons propagating in magnetic fields in spiral galaxies has been used to generate a spectrum of synchrotron radiation. This has in turn been integrated over the entire sky, taking into account the evolution of the sources with redshift, their overall density in the Universe and two different models for the strength of the synchrotron emission for an average spiral galaxy. The result is that, using optimistic assumptions for the undetermined parameters and an average galactic synchrotron luminosity somewhat larger than might be expected from more complete surveys of radio fluxes, it is possible that normal synchrotron radiation might be responsible. The need for optimistic assumptions does unfortunately make this scenario less plausible than one might hope, though they are not a case for exclusion either. However, the fact that such a simple model has a chance of being successful is a small victory in itself. If nothing else had been achieved, that would still be an interesting accomplishment. Furthermore, it should be noted that even for a case where normal spiral galaxies contribute only a large percentage of ARCADE, the excess can be accommodated. This is because some of the excess can already be accounted for by point sources (see Figure 3.1). Hence the ARCADE excess might be the sum of these contributions. If this is indeed the case, one would need somewhat less optimistic assumptions for the normalization parameters.

Additionally, an independent test was done to check the viability of the redshift evolution of the sources. This was accomplished by calculating the angular correlation function corresponding to the type of sources considered. While failing somewhat at larger scales, the model was found to reproduce the expected behavior. In particular, this was found to be not very sensitive to the choice of parameters.

The main point to take away seems to be that more complete knowledge of extra-galactic astrophysics is required to make any conclusive judgment. In particular a better knowledge of cosmic rays, magnetic fields and the synchrotron flux of normal spiral galaxies, as well as the redshift evolution of these sources, is needed. In general it is prudent to gain as complete knowledge of the astrophysical background as possible, before venturing to the more exotic ideas like dark matter. While presently it seems almost certain that dark matter exists and finding new ways to look for traces of it is quite helpful, it should be noted that looking in the wrong place is certainly not desirable. With this in mind, it might be sensible to prioritize more conventional scenarios. In other words, one should perhaps set dark matter aside while ordinary astrophysical scenarios have yet to be explored.

4.1 Outlook

As indicated above, the main way to proceed with this line of inquiry would be to get better or more constraining data to either conclusively rule, out or further motivate, the idea of this thesis. It is acknowledged that some more data might already be available, but it was not found in the time set aside for the work. Further studies might therefore attempt more thorough literature searches and try to get better statistics with regards to some of the parameters and other choices made when building the model used in the thesis. In particular, a more definite value for the average density of galaxies could be derived by studying the luminosity functions of large catalogs. This could also give a more precise estimate on the fraction of spiral galaxies. If a luminosity function representative of spiral galaxies in the Universe is found, one might derive a value for the overall normalization with more confidence. Furthermore, since the utilized model is so simple, a more intricate model could be made in order to gain higher accuracy.

Appendix A:

Variation of the electron spectral index and the magnetic field strength

As noted in Chapter 3, neither the electron spectral nor the magnetic field strength are parameters that can be varied within the model used. Rather, they are set by hand specifically to get the best possible fit to the ARCADE excess. Hence, the effect of varying these parameters was not shown in the text proper. However, since changing either of the two has a very noticeable impact on the result, some additional plots showing this will be displayed here. The other parameter values chosen to demonstrate this are the ones in Figure 3.13, specifically for the case with $z_{\mathrm{p}} = 2$ and $\beta = 2$. The expected behavior is that the electron spectral index will change the synchrotron spectral index, and consequently also change the slope of the intensity. Using different values for the magnetic field strength should move the spectrum right or left (right for higher values and left for smaller ones). This is because changing the magnetic field strength changes the critical frequency.

Starting with the magnetic field strength, the variation in the synchrotron intensity compared with the base case and the ARCADE excess is shown in Figure A.1 and Figure A.2. This is as expected. There is quite some difference for the lowest two values, while the rest are very similar. This seems to suggest that a magnetic field strength higher than 2 μG is required, but a few μG above or below 10 is mostly fine. The difference between the chosen value and the ones that give similar results, is the normalization at various points. Since the normalization was fixed by integration, the value at any given frequency differs, while the overall normalization for the whole interval is the same. The field strength 10 μG gives the best fit to ARCADE and was therefore used in the model.

Next, some plots for various values of p are shown in Figure A.3 and Figure A.4. It is clear that the slopes are all wrong to some extent. While it seems (in particular from the $p = 2.0$ case) that the sensitivity is not strong enough to demand that p should be exactly 2.24, there is no compelling reason to set it to any other value either. In any case, the normalization at various frequencies changes also in this case (for the same reason as above). It is evident that the value preferred from considering the slope, also gives the best fit to ARCADE for the normalization. Thus, the value $p = 2.24$ can be set in the model with some confidence.

From the above considerations it can be concluded that, while there is in principle some freedom

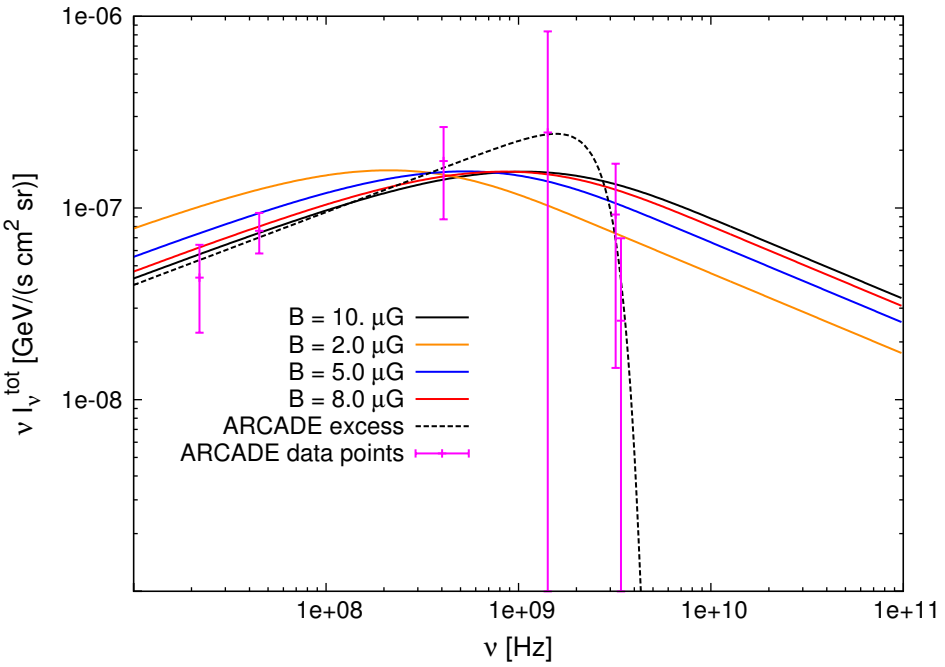

Figure A.1: Synchrotron intensity with varying magnetic field strength compared with ARCADE (dashed black line), showing the base case of 10 μG (solid black line), 2 μG (orange line), 5 μG (blue line) and 8 μG (red line). Also shown are computed data points (magenta).

in choosing values slightly higher or lower, the model demands certain values for these two parameters in order to fit well with ARCADE. This constrains the applicability of the model somewhat, but since only average values are considered (clearly all spiral galaxies do not have the same values for these parameters), the model is not invalidated in any way. This is another case where better experimental data for the values of these parameters in different galaxies would be beneficial, in order make any conclusive statements on the credibility of the model used in this thesis.

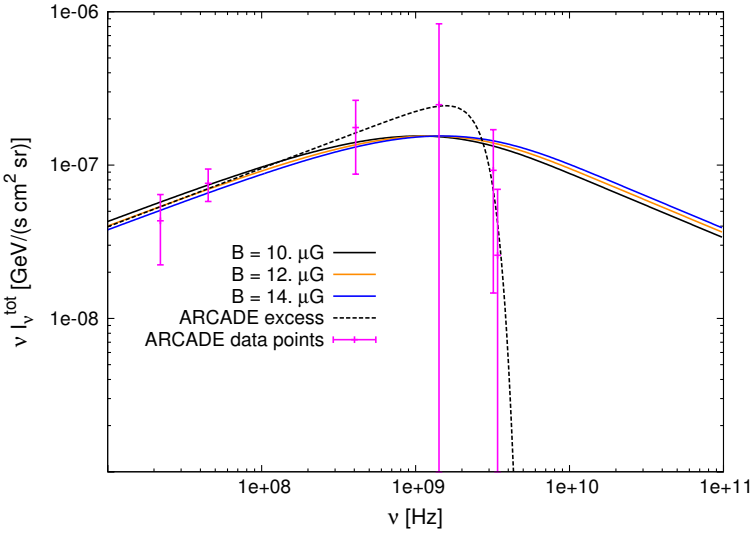

Figure A.2: Synchrotron intensity with varying magnetic field strength compared with ARCADE (dashed black line), showing the base case of 10 μG (solid black line), 12 μG (orange line) and 14 μG (blue line). Also shown are computed data points (magenta).

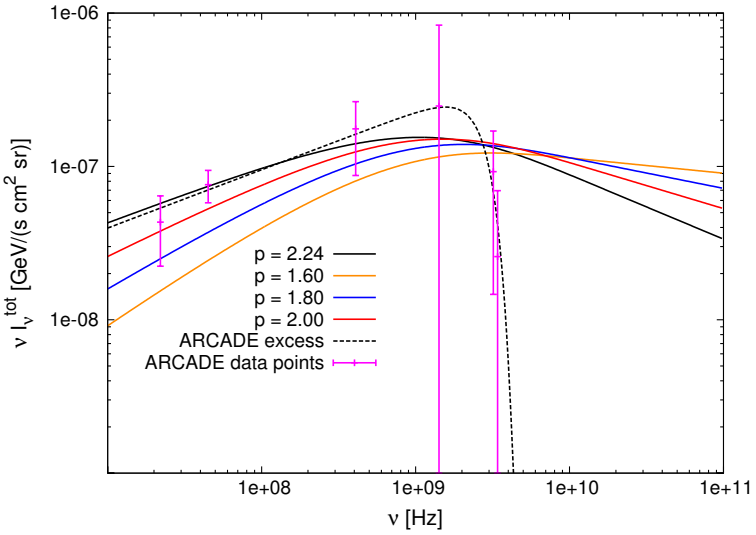

Figure A.3: Synchrotron intensity with varying electron spectral index p, compared with ARCADE (dashed black line). Showing the base case of 2.24 (solid black line), 1.6 (orange line), 1.8 (blue line) and 2.0 (red line). Also shown are computed data points (magenta).

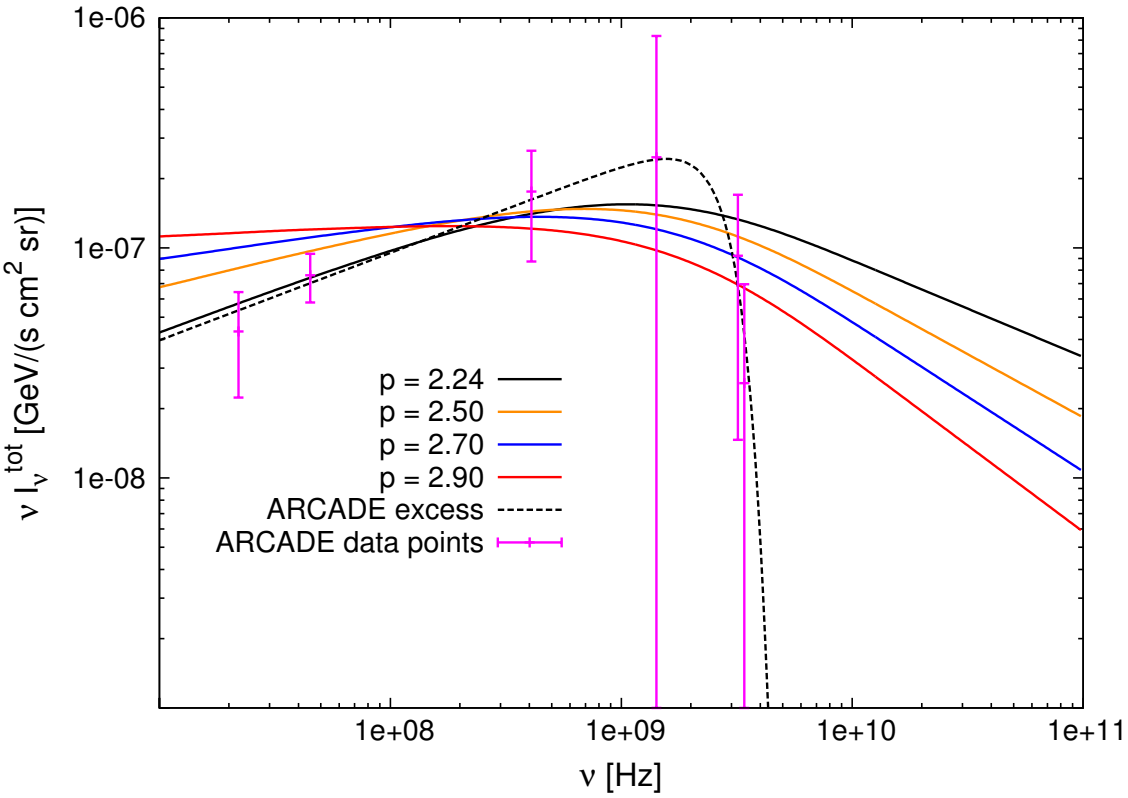

Figure A.4: Synchrotron intensity with varying electron spectral index p, compared with ARCADE (dashed black line). Showing the base case of 2.24 (solid black line), 2.5 (orange line), 2.7 (blue line) and 2.9 (red line). Also shown are computed data points (magenta).

Bibliography

[1] A. Albrecht and P. J. Steinhardt. 'Cosmology for Grand Unified Theories with Radiatively Induced Symmetry Breaking'. *Physical Review Letters*, 48:1220, 1982.

[2] J. Alvarez-Muñiz and T. Stanev. 'The Large Scale Structure of the Galactic Magnetic Field and High Energy Cosmic Ray Anisotropy'. *Journal of Physics: Conference Series*, 47:126, 2006.

[3] W. I. Axford, E. Leer, and G. Skadron. 'The Acceleration of Cosmic Rays by Shock Waves'. *15th Internation Cosmic Ray Conference, Conference Papers*, 11:132, 1978.

[4] A. Basu and S. Roy. 'Magnetic fields in nearby normal galaxies: Energy equipartition'. *arXiv:1305.2746 [astro-ph.GA]*, 2013.

[5] R. Beck. 'Galactic and extragalactic magnetic fields – a concise review'. *Astrophysics and Space Science Transactions*, 5:43, 2009.

[6] J. D. Bekenstein. 'Relativistic gravitation theory for the modified Newtonian dynamics paradigm'. *Physical Review D*, 70:083509, 2004.

[7] A. R. Bell. 'The acceleration of cosmic rays in shock fronts. I'. *Monthly Notices of the Royal Astronomical Society*, 182:147, 1978.

[8] G. Bertone et al. *Particle Dark Matter*. Cambridge University Press, 2010.

[9] G. Bertone, D. Hooper, and J. Silk. 'Particle dark matter: evidence, candidates and constraints'. *Physics Reports*, 405:279, 2005.

[10] R. D. Blandford and J. P. Ostriker. 'Particle acceleration by astrophyscial shock fronts'. *Astrophysical Journal*, 221:L29, 1978.

[11] G. Bothun. *Modern Cosmological Observations and Problems*. Taylor & Francis Ltd, 1998.

[12] T. Bringmann, F. Donato, and R. A. Lineros. 'Radio data and synchrotron emission in consistent cosmic ray models'. *Journal of Cosmology and Astroparticle Physics*, 01:049, 2012.

[13] J. J. Condon. 'A 1.49 GHz Survey of Spiral Galaxies with $B_T \leq +12$ and $\delta \geq -45^{\circ}$'. *The Astrophysical Journal Supplement Series*, 65:485, 1987.

[14] J. J. Condon. 'Radio Emission From Normal Galaxies'. *Annual Review of Astronomy and Astrophysics*, 30:575, 1992.

[15] D. Crowe et al. 'A Direct Empirical Proof of the Existence of Dark Matter'. *The Astrophysical Journal*, 648:L109, 2006.

[16] J. L. Feng. 'Dark Matter Candidates from Particle Physics and Methods of Detection'. *arXiv:1003.0904 [astro-ph CO]*, 2010.

[17] E. Fermi. 'On the Origin of the Cosmic Radiation'. *Physical Review*, 75:1196, 1949.

[18] D. J. Fixsen et al. 'ARCADE 2 Measurement of the Extra-Galactic Sky Temperature at 3-90 GHz'. *arXiv:0901.0555v1 [astro-ph.CO]*, 2009.

[19] N. Fornengo, R. Lineros, M. Regis, and M. Taoso. 'Possibility of a Dark Matter Interpretation for the Excess in Isotropic Radio Emission Reported by ARCADE'. *Physical Review Letters*, 107:271302, 2011.

[20] N. Fornengo, R. Lineros, M. Regis, and M. Taoso. 'Cosmological radio emission induced by WIMP Dark Matter'. *Journal of Cosmology and Astrophysics*, 03:033, 2012.

[21] N. Fornengo, R. Lineros, M. Regis, and M. Taoso. 'Galactic synchrotron emission from WIMPs at radio frequencies'. *Journal of Cosmology and Astrophysics*, 01:005, 2012.

[22] K. Greisen. 'End to the Cosmic Ray Spectrum?'. *Physical Review Letters*, 16:748, 1966.

[23] K. Griest. 'Galactic Microlensing as a Method of Detecting Massive Compact Halo Objects'. *The Astrophysical Journal*, 366:412, 1991.

[24] A. H. Guth. 'Inflationary Universe: A possible solution to the horizon and flatness problems'. *Physical Review D*, 23:347, 1981.

[25] J. D. Jackson. *Classical Electrodynamics*. John Wiley & Sons, Inc., third edition, 1999.

[26] K. Nakamura et al. (Particle Data Group). 'Review of Particle Physics'. *Journal of Physics G: Nuclear and Particle Physics*, 37(7A), 2010.

[27] T. Kaluza. 'Zum Unitätsproblem der Physik'. *Sitzungsber. Preuss. Akad. Wiss. Berlin. (Math. Phys.)*, 1921:966, 1921.

[28] O. Klein. 'Quantentheorie und fünfdimensionale Relativitätstheorie'. *Zeitschrift für Physik*, 37:895, 1926.

[29] A. Kogut et al. 'An Instrument to Measure the Temperature of the Cosmic Microwave Background Radiation at Centimeter Wavelengths'. *The Astrophysical Journal Supplemental Series*, 154:493, 2004.

[30] A. Kogut et al. 'ARCADE 2 Observations Of Galactic Radio Emission'. *The Astrophysical Journal*, 734:4, 2011.

[31] E. W. Kolb and M. S. Turner. *The Early Universe*. Addison-Wesley Publishing Company, 1990.

[32] G. F. Krysmky. 'A regular mechanism for the acceleration of charged particles on the front of a shock wave'. *Doklady Akademiya Nauk SSSR*, 234:1306, 1977.

[33] A. Letessier-Selvon and T. Stanev. 'Ultrahigh Energy Cosmic Rays'. *Review of Modern Physics*, 83:907, 2011.

[34] A. D. Linde. 'A New Inflationary Universe Scenario: A Possible Solution Of The Horizon, Flatness, Homogeneity, Isotropy And Primordial Monopole Problems'. *Physics Letters B*, 108:389, 1982.

[35] C. Lintott et al. 'Galaxy Zoo 1: data release of morphological classifications for nearly 900 000 galaxies'. *Monthly Notices of the Royal Astronomical Society*, 410:166, 2011.

[36] M. S. Longair. *High Energy Astrophysics*. Cambridge University Press, third edition, 2011.

[37] M. Milgrom. 'A Modification of the Newtonian Dynamics As A Possible Alternative to the Hidden Mass Hypothesis'. *The Astrophysical Journal*, 270:365, 1983.

[38] M. Milgrom. 'A Modification of the Newtonian Dynamics: Implications For Galaxies'. *The Astrophysical Journal*, 270:371, 1983.

[39] C. W. Misner, K. S. Thorne, and J. A. Wheeler. *Gravitation*. W. H. Freeman and Company, 1973.

[40] NASA/WMAP Science Team. `http://map.gsfc.nasa.gov/media/121238/index.html`, 2012.

[41] S. Niklas, U. Klein, and R. Wielebinski. 'A radio continuum survey of shapley-ames galaxies at λ 2.8 cm. I. Atlas of radio data'. *Astronomy and Astrophysics Supplement Series*, 114:21, 1995.

[42] S. Niklas, U. Klein, and R. Wielebinski. 'A radio continuum survey of shapley-ames galaxies at λ 2.8 cm. II. Separation of thermal and non-thermal radio emission'. *Astronomy and Astrophysics*, 322:19, 1997.

[43] J. P. Ostriker and P. J. E. Peebles. 'A Numerical Study of the Stability of Flattened Galaxies: Or Can Cold Galaxies Survive?'. *The Astrophysical Journal*, 186, 1973.

[44] J. P. Ostriker, P. J. E. Peebles, and A. Yahil. 'The Size and Mass of Galaxies, and the Mass of the Universe'. *The Astrophysical Journal*, 193:L1-L4, 1974.

[45] R. D. Peccei and H. R. Quinn. 'Constraints Imposed by CP Conservation in the Presence of Pseudoparticles'. *Physical Review D*, 16:1791, 1977.

[46] R. D. Peccei and H. R. Quinn. 'CP Conservation in the Presence of Pseudoparticles'. *Physical Review Letters*, 38:1440, 1977.

[47] S. Perlmutter et al. 'Measurements of Ω and Λ From 42 High-Redshift Supernovae'. *The Astrophysical Journal*, 517:565, 1999.

[48] A. M. Polyakov. 'Particle spectrum in quantum field theory'. *Journal of Experimental and Theoretical Physics Letters*, 20:194, 1974.

[49] J. P. Preskill. 'Cosmological Production of Superheavy Magnetic Monopoles'. *Physical Review Letters*, 43:1365, 1979.

[50] A. G. Riess et al. 'Observational Evidence From Supernovae For An Accelerating Universe and A Cosmological Constant'. *The Astronomical Journal*, 116:1009, 1998.

[51] J. Robert C. Kennicutt. 'Star Formation in Galaxies Along the Hubble Sequence'. *Annual Review of Astronomy and Astrophysics*, 36:189, 1998.

[52] V. C. Rubin and J. W. Kent Ford. 'Rotation of the Andromeda Nebula from a Spectroscopic Survey of Emission Regions'. *The Astrophysical Journal*, 159, 1970.

[53] V. C. Rubin, J. W. Kent Ford, and N. Thonnard. 'Extended Rotation Curves of High Luminosity Spiral Galaxies. IV. Systematic Dynamical Properties Sa→Sc'. *The Astrophysical Journal*, 225:L107-L111, 1978.

[54] V. Sahni. Dark matter and dark energy. *arXiv:astro-ph/0403324*, 2004.

[55] A. Sandage and G. A. Tammann. *A Revised Shapley-Ames Catalog of Bright Galaxies*. Carnegie Institution of Washington, 1981.

[56] M. Seiffert et al. 'Interpretation of the ARCADE 2 Absolute Sky Brightness Measurement'. *The Astrophysical Journal*, 734:6, 2011.

[57] M. M. Shapiro, T. Stanev, and J. P. Wefel. *Astrophysical Sources of High Energy Particles and Radiation (NATO Science Series)*. Kluwer Academic Publishers, 2001.

[58] J. Singal et al. 'The ARCADE 2 Instrument'. *The Astrophysical Journal*, 730(2), 2011.

[59] J. Singal, Ł. Stawarz, A. Lawrence, and V. Petrosian. 'Sources of the radio background considered'. *Monthly Notices of the Royal Astronomical Society*, 409:1172, 2010.

[60] T. Stanev. *High Energy Cosmic Rays*. Springer-Praxis, 2nd edition, 2004.

[61] L. E. Strigari, J. F. Beacom, T. P. Walker, and P. Zhang. 'The concordance cosmic star formation rate: implications from and for the supernova neutrino and gamma ray backgrounds'. *Journal of Cosmology and Astroparticle Physics*, 04:017, 2005.

[62] G. 't Hooft. 'Magnetic Monopoles in Unified Gauge Theories'. *Nuclear Physics B*, 79:276, 1974.

[63] G. 't Hooft. 'Symmetry Breaking through Bell-Jackiw Anomalies'. *Physical Review Letters*, 37:8, 1976.

[64] M. Taoso, G. Bertone, and A. Masiero. 'Dark matter candidates: a ten point test'. *Journal of Cosmology and Astrophysics*, 0803:022, 2008.

[65] M. Tegmark et al. 'The Three-Dimensional Power Spectrum of Galaxies from the Sloan Digital Sky Survey'. *The Astrophysical Journal*, 606:702, 2004.

[66] W. R. Webber and P. R. Higbie. 'Limits on the interstellar cosmic ray electron spectrum below ~ 1-2 GeV derived from the galactic polar radio spectrum and constrained by new Voyager 1 measurements'. *Journal of Geophysical Research: Space Physics*, 113:A11106, 2008.

[67] S. Weinberg. 'A New Light Boson?'. *Physical Review Letters*, 40:223, 1978.

[68] F. Wilczek. 'Problem of Strong P and T Invariance in the Presence of Istantons'. *Physical Review Letters*, 40:279, 1978.

[69] G. T. Zatsepin and V. A. Kuz'min. 'Upper Limit of the Spectrum of Cosmic Rays'. *Journal of Experimental and Theoretical Physics Letters*, 4:78, 1966.

[70] Y. B. Zeldovich and M. Y. Khlopov. 'On the Concentration Of Magnetic Monopoles in the Universe'. *Physics Letters B*, 79:239, 1978.

[71] F. Zwicky. 'Die Rotverschiebung von extragalaktischen Nebeln'. *Helvetica Physica Acta*, 6, 1933.